Nano Research Energy

ISSN 2791-0091 CN 10-1944/O6
https://doi.org/10.26599/NRE.2026.9120293

Review Article

From Crystalline Structure Design to Amorphous Superionic Transport in Sodium Halide Solid Electrolytes: A Mini Review

Huanzhu Lv[1], Shuting Kong[1], Yanbo Li[1], Yu Liu[1], Hanbo Yang[1], Zhengwei Huang[1], Yujie Yan[1], Yingzhi Li[1], Yun Yan[2], Xingqun Liao[2], Zhouguang Lu[1](✉)

[1] Department of Materials Science and Engineering, Southern University of Science and Technology, Shenzhen 518055, China

[2] SUSTech MSE - Highpower Technology Joint Laboratory of New Energy Technology, Shenzhen Highpower Technology Co., Ltd., Shenzhen 518111, China

Nano Research Energy, **Just Accepted Manuscript** • https://doi.org/10.26599/NRE.2026.9120293

https://www.sciopen.com/journal/2791-0091 on Nov. 23, 2026

© The Authors(s)

Just Accepted

This is a "Just Accepted" manuscript, which has been examined by the peer-review process and has been accepted for publication. A "Just Accepted" manuscript is published online shortly after its acceptance, which is prior to technical editing and formatting and author proofing. Tsinghua University Press (TUP) provides "Just Accepted" as an optional and free service which allows authors to make their results available to the research community as soon as possible after acceptance. After a manuscript has been technically edited and formatted, and the page proofs have been corrected, it will be removed from the "Just Accepted" web site and published officially with volume and article number (e.g., Nano Research Energy, 2025, 4, e9120191). Please note that technical editing may introduce minor changes to the manuscript text and/or graphics which may affect the content, and all legal disclaimers that apply to the journal pertain. In no event shall TUP be held responsible for errors or consequences arising from the use of any information contained in these "Just Accepted" manuscripts. To cite this manuscript please use its Digital Object Identifier (DOI®), which is identical for all formats of publication.

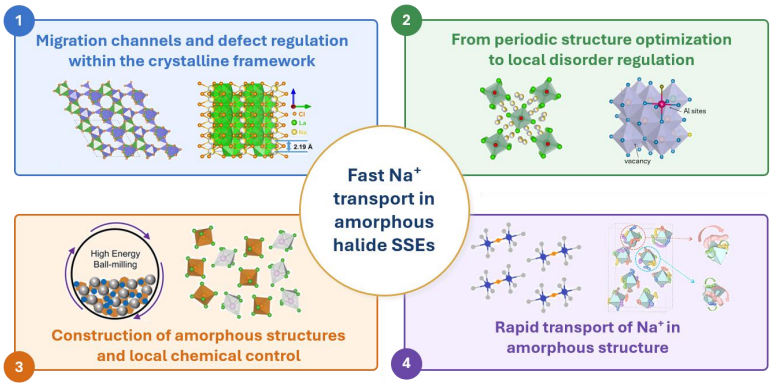
Just Accepted

From Crystalline Structure Design to Amorphous Superionic Transport in Sodium Halide Solid Electrolytes: A Mini Review

Huanzhu Lv[1], Shuting Kong[1], Yanbo Li[1], Yu Liu[1], Hanbo Yang[1], Zhengwei Huang[1], Yujie Yan[1], Yingzhi Li[1], Yun Yan[2], Xingqun Liao[2], Zhouguang Lu[1*]

[1]Department of Materials Science and Engineering, Southern University of Science and Technology, Shenzhen, 518055, Guangdong, P. R. China.

[2]SUSTech MSE - Highpower Technology Joint Laboratory of New Energy Technol-ogy, Shenzhen Highpower Technology Co., Ltd., Shenzhen 518111, Guangdong, P. R. China.



This review summarizes the evolution of sodium halide solid-state electrolytes, ranging from the optimization of crystalline frameworks to the design of amorphous structures, with a particular focus on the roles of local coordination, connectivity, configurational degrees of freedom, and framework dynamics in modulating Na^+ transport. Furthermore, the article discusses the key challenges and future opportunities associated with developing amorphous sodium halide electrolytes that allow for quantitative description and predictive design, and are suitable for battery systems.

Just Accepted

Nano Research Energy

ISSN 2791-0091 (print); 2790-8119 (online)
https://doi.org/10.26599/NRE.2026.9120293

Review Article

From Crystalline Structure Design to Amorphous Superionic Transport in Sodium Halide Solid Electrolytes: A Mini Review

Huanzhu Lv[1], Shuting Kong[1], Yanbo Li[1], Yu Liu[1], Hanbo Yang[1], Zhengwei Huang[1], Yujie Yan[1], Yingzhi Li[1], Yur Yan[2], Xingqun Liao[2], and Zhouguang Lu[1] (✉)

[1] *Department of Materials Science and Engineering, Southern University of Science and Technology, Shenzhen 518055, China*
[2] *SUSTech MSE - Highpower Technology Joint Laboratory of New Energy Technology, Shenzhen Highpower Technology Co., Ltd Shenzhen 518111, China*

© The Author(s) 2026

Received: 27 September 2026 / **Revised:** 22 October 2026 / **Accepted:** 2 November 2026

ABSTRACT

Halide solid-state electrolytes, owing to their relatively high electrochemical stability, favorable mechanical compressibility, and broad compositional tunability, are emerging as an important class of electrolytes for all-solid-state sodium-ion batteries (ASSIBs). Compared with Li^+, the larger Na^+ ion is more sensitive to local coordination and available migration space, making it difficult for strategies based solely on channel dimensions, site occupancy, and defect concentration in crystalline frameworks to simultaneously ensure structural stability and fast ion transport. Accordingly, structural design in sodium halides is shifting from optimization of static migration channels in periodic lattices toward regulation of local coordination disorder, structural connectivity, and framework dynamics, with amorphization providing an important route to overcome crystallographic constraints. This Mini Review first discusses the regulation of migration pathways, metastable sites, and defect networks in crystalline sodium halides and how these concepts have progressively shifted the design focus from average periodic structures to local environments. It then highlights how mechanochemistry, compositional tuning, mixed-anion chemistry, and rapid quenching regulate amorphous-phase formation, local coordination, short-range connectivity, and multiphase microstructures. On this basis, we further discuss how local connectivity, structural coherence, configurational freedom, and framework dynamics collectively shape the Na^+ migration energy landscape in amorphous structures. Current evidence indicates that amorphization itself is not sufficient to ensure fast Na^+ transport. More critically, local coordination constraints must be weakened while interconnected low-barrier migration configurations are established, without allowing excessive short-range structural coherence to reimpose configurational restrictions; transient rearrangements of flexible frameworks may further reduce local constraints during migration. Finally, we outline key directions including quantitative description and controllable construction of amorphous structures, causal elucidation of static disorder and dynamic transport, predictive materials design, and translation to battery-scale performance. A central scientific question is how local structural connectivity, configurational freedom, and framework dynamics can be rationally regulated to establish continuous low-barrier Na^+ migration pathways in amorphous sodium halide electrolytes. Addressing this question is essential for advancing sodium halide electrolytes from empirical amorphization toward predictable structure-guided design.

KEYWORDS

sodium halide solid electrolytes, amorphous structures, superionic transport, structure–transport relationships

1 Introduction

All-solid-state sodium-ion batteries (ASSIBs) are widely regarded as a promising energy-storage technology that combines resource sustainability with improved safety, and solid-state electrolytes (SSEs) with high Na^+ conductivity, favorable electrochemical stability, and good electrode compatibility are essential for their high-performance operation [1-9]. Current inorganic sodium-ion SSEs are dominated by oxides [10-12], sulfides [13-15], and halides [16, 17]. Oxide SSEs generally exhibit good chemical and thermal stability, but their high elastic moduli and substantial grain-boundary resistance make intimate interfacial contact at room temperature challenging. Sulfide SSEs offer high ionic conductivity and good mechanical compressibility, yet their air sensitivity

© The Author(s) 2027. Published by Tsinghua University Press. The articles published in this open access journal are distributed under the terms of the Creative Commons Attribution 4.0 International License (http://creativecommons.org/licenses/by/4.0/), which permits use, distribution and reproduction in any medium, provided the original work is properly cited.

Address correspondence to Zhouguang Lu, luzg@sustech.edu.cn

TSINGHUA UNIVERSITY PRESS SciOpen

and limited high-voltage stability complicate material processing and cell integration. In comparison, halides provide a broad compositional design space, favorable compatibility with high-voltage cathodes, and relatively soft lattices, making them an attractive electrolyte platform for high-voltage ASSIBs [18-20].

The relatively large ionic radius of Na^+ makes its migration through solid frameworks particularly sensitive to local free volume, coordination environment, and structural connectivity [21]. Early design of sodium halides largely followed classical crystal-chemical principles, in which suitable anion frameworks, lattice dimensions, aliovalent substitution, and Na^+ vacancies were used to optimize migration pathways within predefined periodic structures [19,22,23]. This approach established fundamental relationships among crystal structure, site occupancy, and ion transport in UCl_3-type [22], rock-salt-type [23], and other chloride frameworks [24,25].

As research progressed, however, it became increasingly clear that average crystal structures alone cannot fully account for the large transport differences among sodium halides. For example, $NaAlCl_4$ can exhibit pronounced changes in Na^+ site occupancy and ionic conductivity after mechanochemical treatment and subsequent annealing while retaining the same average space group [26]. In $LaCl_3$-type halides, ball milling can likewise alter metastable site occupancy and local defect states without substantially disrupting the parent framework [22]. Similarly, stoichiometrically identical $NaNbOCl_4$ can acquire different degrees of short- and long-range order simply by changing the melt-cooling rate, resulting in markedly different Na^+ transport behavior [27]. These observations show that fast ion transport is governed not only by lattice-scale channel geometry and average vacancy concentration, but also by metastable-site occupation [22,24], the spatial distribution of defects [23], local coordination distortion, and connectivity between short-range structural units [27-29]. This recognition has shifted sodium-halide research from optimization of periodic lattices toward control of local disorder. Mixed-anion chemistry can directly modify the first coordination shells of metal centers and Na^+ and reconstruct local networks through bridging or non-bridging connections [28,30-32], whereas multication and high-entropy strategies broaden the distributions of local coordination environments and site energies and promote exchange between distinct Na^+ sites [33]. Meanwhile, mechanochemical processing can generate structural states ranging from nanocrystalline-amorphous coexistence to highly amorphous phases [34-36]; rapid quenching can freeze different degrees of short-range order by suppressing structural relaxation and crystallization [27]; and reactive precursors such as carbonates and borates can substantially alter both the pathway and rate of amorphous-phase formation [31,32].

Importantly, loss of long-range order does not imply complete randomization of local structure. X-ray absorption spectroscopy (XAS), pair distribution function (PDF) analysis, Raman spectroscopy, solid-state nuclear magnetic resonance (NMR), and atomistic simulations of various amorphous sodium halides show that metal-halide/oxygen coordination polyhedra and their short-range connections can persist to different extents even after long-range periodicity has largely disappeared [27,29,31,32,34,35]. What changes most substantially are often the coordination numbers, degrees of distortion, orientational relationships, and connection modes of these local units. Thus, “amorphization” is not a unique structural or transport descriptor. More fundamental questions are which local structures are retained or reconstructed during amorphization, how these local units form continuous Na^+ migration networks, and whether the resulting structural degrees of freedom can further reduce transient migration constraints through dynamic responses.

The recent emergence of highly conductive amorphous and strongly disordered sodium halides has further reshaped the understanding of the relationship between structural disorder and Na^+ transport [27,28,31,32,34,35]. Some materials exhibit room-temperature ionic conductivities in the mS cm^{-1} range and low migration activation energies after losing long-range periodicity, yet pronounced transport differences remain among amorphous systems, demonstrating that disruption of long-range order alone does not guarantee rapid diffusion [27-29,36]. Even among materials with similar amorphous signatures, Na^+ local coordination, connectivity between neighboring polyhedra, and residual short-range structural correlations can differ markedly, giving rise to distinct site-energy distributions and migration networks. Increasingly, atomistic studies are therefore attributing these transport differences to specific local structures and dynamic processes: local polyhedral connectivity, structural coherence, and the range of accessible configurations collectively determine the migration potential-energy landscape experienced by Na^+, while weaker local binding and more continuous low-energy configurations favor the establishment of long-range diffusion pathways. At the same time, flexible anionic or polyhedral frameworks are not passive backgrounds. Their thermally activated reorientation, vibration, and local relaxation can continuously modify the instantaneous coordination and migration bottlenecks around Na^+, rendering the migration environment intrinsically time dependent [32,37,38]. Fast ion transport in amorphous sodium halides is thus increasingly understood as the combined outcome of local structure, migration-network connectivity, and dynamic framework response rather than as a simple consequence of the loss of long-range order [29,32,37].

Just Accepted

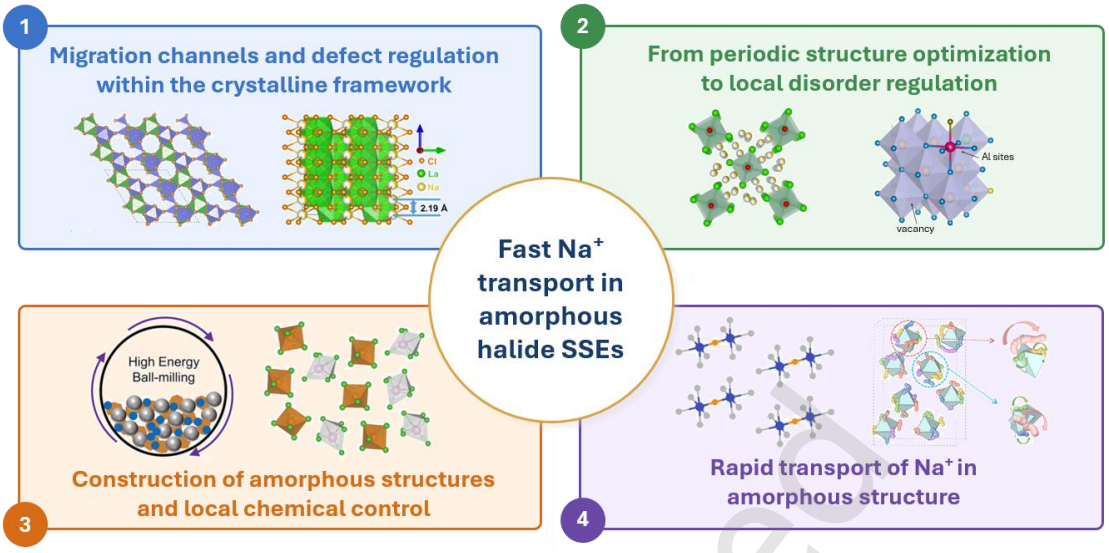


Figure 1. Evolution of structural design concepts for sodium halide solid electrolytes from crystalline frameworks to amorphous superionic transport. The structural illustrations are adapted with permission from Refs. [22,29,30,34,37,39], published by Springer Nature ([22,37]), Wiley-VCH ([29,30]), the American Chemical Society ([39]), and Elsevier ([34]).

2 From Crystalline Frameworks to Structural Disorder: Evolution of Design Concepts in Sodium Halides

The study of sodium halide SSE was originally rooted in crystal chemistry, with well-resolved crystal structures explaining Na^+ occupancy and migration. From the perspective of structural organization, sodium halide SSE can be roughly divided into crystalline systems, partially disordered or multiphase systems, and amorphous systems. The main differences lie in their long-range periodicity, local structural disorder, and phase characteristics. Since relatively large Na^+ ions are sensitive to local free volume and coordination, a core challenge in materials design has long been to establish continuous low-barrier migration paths within a structurally stable framework. However, as more sodium halide systems were reported, the relationship between ion transport and crystal structure proved to be more complex than initially expected. Materials with similar parent structures can exhibit significantly different ionic conductivities, while mechanochemical treatments and small compositional changes can significantly alter transport behavior. Therefore, understanding structural factors beyond the average crystal structure has become an increasingly important issue in sodium halide SSE research [16,18].

2.1 Migration Pathways and Defect Regulation in Crystalline Frameworks

Early design of crystalline sodium halides largely followed the structural-chemistry principles established for classical fast-ion conductors: the anion framework defines the crystallographic sites accessible to Na^+ and the possible migration directions, while transport is further governed by migration bottlenecks, site occupancy, and vacancy concentration. Because of the large Na^+ radius, limited free volume in halide frameworks can readily become a transport constraint, and early studies therefore focused on identifying favorable crystal topologies and tuning accessible Na^+ pathways within predefined periodic structures. $NaAlCl_4$ provides a representative example [26]. Unlike common chlorides built from MCl_6 octahedra, Al^{3+} in $NaAlCl_4$ forms isolated $AlCl_4^-$ tetrahedra, with Na^+ occupying prismatic coordination environments between them. Mechanochemically prepared BM-$NaAlCl_4$ (BM, ball-milled) exhibits an ionic conductivity of 3.9×10^{-6} S cm^{-1} at 30 °C and an activation energy of 0.42 eV. After annealing at 200 °C to increase crystallinity, the conductivity decreases to 3.3×10^{-7} S cm^{-1}, although all samples remain assignable to the orthorhombic $P2_12_12_1$ structure. Structural refinement further reveals changes in Na^+ site occupation associated with crystallinity. In BM-$NaAlCl_4$, Na^+ is distributed over two prismatic sites, Na1 and Na2, whereas highly crystalline HT200-$NaAlCl_4$ (HT200, heat-treated at 200 °C) is better described by a model without Na2 occupancy (Fig. 2a, b). Although the configuration with all Na^+ ions on Na1 is computationally more stable, the energy differences among alternative occupation models are only 5-53 meV atom^{-1}, allowing mechanochemical processing to stabilize the additional Na2 site. Bond-valence energy landscape (BVEL) calculations identify three Na1/Na2 hopping modes, with migration through the larger rectangular face being substantially more favorable than through the smaller triangular face. These hops first form one-dimensional channels along [001] and are extended through Na2 sites into a two-dimensional migration network in the ac plane. Thus, even without changing the space group, mechanochemically induced nonequilibrium site occupancy can alter the connectivity of the migration network (Fig. 2d).

$LaCl_3$-type systems subsequently extended this strategy by directly tuning crystal topology [22]. $NaLaCl_4$ adopts a $P6_3/m$ UCl_3-type framework (Fig. 2e), in which Na^+ migrates mainly through one-dimensional hexagonal channels along the c axis. Ion transport in the unsubstituted framework is nevertheless sluggish,

Just Accepted

showing that the mere presence of a channel does not guarantee low-barrier migration. Substitution of La^{3+} by Zr^{4+} introduces shorter Zr-Cl bonds and modifies the local channel geometry. Both calculations and X-ray absorption fine structure (XAFS) measurements indicate that the Na-Cl distance increases from approximately 2.87 to 2.91 Å, widening the diffusion bottleneck and lowering the site energy near the bottleneck (Fig. 2c, f, h, i). The calculated migration barrier correspondingly decreases from approximately 0.26 eV in $NaLaCl_4$ to about 0.04 eV in the substituted system. Mechanochemical treatment produces an additional effect by enabling greater Zr solubility and introducing antisite and related defects. The occupancy of Na^+ at the metastable 2b site increases from approximately 0.16 in the heat-treated sample to 0.251 in the ball-milled sample, while the long-range UCl_3-type framework remains largely intact. Optimized $Na_{0.7}Zr_{0.3}La_{0.7}Cl_4$ reaches 2.9×10^{-4} S cm^{-1} at 30 °C with an activation energy of 0.33 eV (Fig. 2g). It should be noted that the calculated migration barrier of 0.04 eV corresponds to Na^+ hopping along a specific local migration pathway within the modeled structure, whereas the experimentally determined activation energy of 0.33 eV reflects the effective thermal activation of macroscopic ionic conduction. Unlike an individual hopping event, long-range Na^+ transport involves successive migrations through interconnected sites and is influenced by the distribution of local site energies, pathway connectivity, and potentially rate-limiting migration steps. Therefore, a low local migration barrier does not necessarily translate into an equally low experimental activation energy. When used as the cathode-side electrolyte with $NaCrO_2$, the resulting ASSIB delivers an initial capacity of 114 mAh g^{-1}, retains 88% of its capacity after 70 cycles at 0.3 C, and still provides approximately 94 mAh g^{-1} at 1 C.

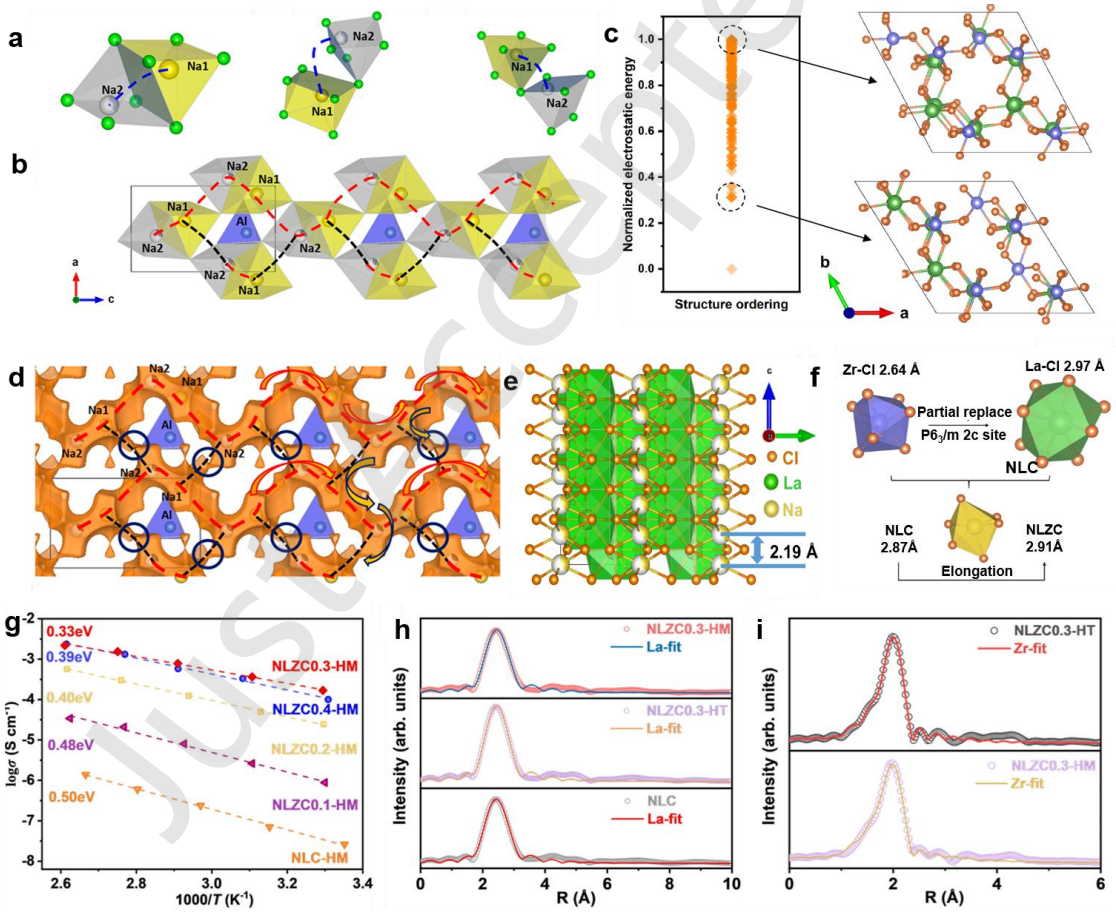


Figure 2 (a) Three representative Na^+ migration mechanisms (transitions I-III) involving Na1 and Na2 sites. (b) Na^+ diffusion pathways identified by bond-valence energy landscape analysis. (c) Normalized electrostatic energies of Na-vacancy configurations in the NLZC supercell, with representative high- and low-energy structures. (d) Bond-valence isosurface map illustrating the extended Na^+ migration network. (e) Crystal structure/Rietveld refinement of the $NaLaCl_4$-based UCl_3-type framework. (f) Local La-Cl, Zr-Cl, and Na-Cl distance changes after Zr substitution. (g) Arrhenius conductivity plots of $NLZC_x$-HM ($0 \le x \le 0.4$). (h, i) Representative La- and Zr-centered coordination environments. (a,b,d) are adapted with permission from Ref. [26], published by the American Chemical Society ; (c, e–i) are adapted with permission from Ref. [22], published by Springer Nature.

From $NaAlCl_4$ to $LaCl_3$-type materials, the design focus progressed from asking whether a lattice possesses Na^+ channels to understanding metastable sites, local bottlenecks, and cation disorder within those channels.

Just accepted

$Na_{2.5}Cr_{0.5}Zr_{0.5}Cl_6$ extends this concept further to the vacancy network [23]. Na_2ZrCl_6 originally adopts a trigonal structure with a hexagonal close-packed (hcp) anion arrangement, whereas adjusting the Cr/Zr ratio to 1:1 yields a cubic $Fm\bar{3}m$ rock-salt phase with a cubic close-packed (ccp) Cl- framework. Na, Cr, Zr, and vacancies occupy approximately 41.67%, 8.33%, 8.33%, and 41.67%, respectively, of the parent NaCl-type cation sites. Its room-temperature ionic conductivity reaches 0.1 mS cm^{-1}, exceeding those of Na_3CrCl_6 (0.0035 mS cm^{-1}) and Na_2ZrCl_6 (0.013 mS cm^{-1}). The high vacancy concentration, however, captures only part of the transport physics. In the lowest-energy supercell, Cr^{3+}, Zr^{4+}, and vacancies exhibit local clustering, and the three-dimensional network derived from BVEL calculations shows pronounced local selectivity: Na^+ transport is favored along connections involving $NaCl_6$ and VCl_6 nodes, whereas $CrCl_6$ and $ZrCl_6$ nodes impose greater migration resistance. Thus, an identical vacancy concentration does not yield an equivalent transport network when vacancies adopt different spatial arrangements. NCZC0.5 also exhibits a low electronic conductivity of approximately 3.8 × 10^{-9} S cm^{-1}, with pronounced oxidative decomposition beginning at about 4.0 V versus Na/Na^+. $Na_{15}Sn_4$ symmetric-cell measurements further confirm its capability for Na^+ transport as an SSE.

These crystalline systems progressively shifted the structure-transport relationship from the average crystal structure toward smaller spatial scales. Although migration-channel dimensionality defines the basic diffusion topology, whether Na^+ occupies metastable positions, whether vacancies form connected networks, and whether aliovalent metal centers create local blocking nodes can all redefine the migration network that is actually accessible. Mechanochemical treatment has therefore become widely used even for high-performance crystalline sodium halides because it can modify site occupancy and local defect configurations without changing the parent space group. The average crystal structure remains an essential descriptor, but it is no longer sufficient on its own to explain ionic conductivity [40].

2.2 From Periodic-Structure Optimization to Local-Disorder Regulation

The structural freedom available from tuning sites and vacancies within the cation sublattice is inherently limited. Mixed-anion systems subsequently expanded this design space by directly modifying the anion framework that defines the migration environment. Differences in charge, polarizability, and coordination preference among O^{2-}, S^{2-}, and Cl^- not only introduce charge compensation but also alter the connectivity between metal-centered coordination units and the first coordination shell of Na^+. Local structure itself thereby becomes an active design variable in sodium halides [41].

In $NaNbCl_{6-2x}O_x$, this evolution is first manifested in changes to metal-anion connectivity [30]. $NaNbCl_6$ adopts a $P2_1/c$ structure containing relatively isolated $NbCl_6$ octahedra. Upon introducing O^{2-}, a characteristic Nb-O-Nb vibration emerges near 788 cm^{-1} in the Raman spectra, consistent with an oxychloride structure containing $[NbCl_4O]$ units. ^{23}Na magic-angle-spinning (MAS) NMR evolves from a single Na environment [42] at approximately -8.1 ppm in $NaNbCl_6$ to an additional signal at -12 to -14 ppm, which becomes dominant in $NaNbCl_4O$ (Fig. 3a). Meanwhile, ^{93}Nb NMR shows enhanced quadrupolar coupling, reflecting a change in the local coordination symmetry around Nb. This local reconstruction is accompanied by a substantial transport enhancement: the room-temperature conductivity increases from approximately 3 × 10^{-6} S cm^{-1} for $NaNbCl_6$ to 1.03 × 10^{-4} S cm^{-1} for $NaNbCl_4O$. Oxygen incorporation does not substantially compromise high-voltage stability, with oxidative decomposition in both compositions beginning near 4.0 V versus Na/Na^+. An ASSIB combining $NaNbCl_4O$ with a layered $Na_{0.7}Fe_{0.3}Mn_{0.65}Al_{0.05}O_2$ cathode delivers approximately 155 mAh g^{-1} at room temperature. Reversible Nb redox is also observed, giving these oxychlorides the dual character of an ionic conductor and a redox-active catholyte.

S^{2-} perturbs the Na-Zr-Cl framework even more strongly [39]. As the sulfur content increases, diffraction peaks of trigonal Na_2ZrCl_6 progressively weaken and cubic reflections assigned to rock-salt Na_3ZrCl_5S emerge. In pure Na_3ZrCl_5S, Na^+, Zr^{4+}, and vacancies occupy approximately 50%, 16.7%, and 33.3% of the cation sites, respectively, while Cl^- and S^{2-} form a mixed-anion sublattice. The structural transition from trigonal to cubic (Fig. 3c) raises the room-temperature conductivity from 0.025 to 0.18 mS cm^{-1} and lowers the activation energy from 0.40 to 0.31 eV. The highest conductivity occurs at the intermediate composition $NZCS_{0.6}$, which contains approximately 54.3 wt.% trigonal phase and 45.7 wt.% cubic phase, while the elevated neutron-diffraction background also indicates an amorphous component. Its room-temperature ionic conductivity reaches 0.753 mS cm^{-1}, approximately 30 times that of pristine Na_2ZrCl_6, with an activation energy of 0.289 eV. Annealing increases crystallinity and decreases the conductivity of all samples, leading the authors to distinguish transport contributions from crystalline interiors, amorphous regions, and crystalline/amorphous interfaces. This structural complexity is also reflected in cell performance. S^{2-} incorporation lowers the oxidative stability from approximately 4.02 V for Na_2ZrCl_6 to approximately 3.63 V versus Na/Na^+ for $NZCS_{0.6}$, revealing a trade-off between conductivity and high-voltage stability, although the resulting window remains compatible with $NaCrO_2$. A $NaCrO_2$ ASSIB using $NZCS_{0.6}$ as the catholyte delivers an initial discharge capacity of 110 mAh g^{-1} at 0.1 C and 75.6 mAh g^{-1} at 1 C; after 1000 cycles at 0.3 C and room temperature, it retains 90.6 mAh g^{-1}, corresponding to 83% capacity retention and an average Coulombic efficiency of approximately 99.95%. In this case, no single "best crystal phase" can account for the high transport performance; rather, the coexistence of multiple structural states and their interfaces become part of the functional transport architecture.

Just Accepted

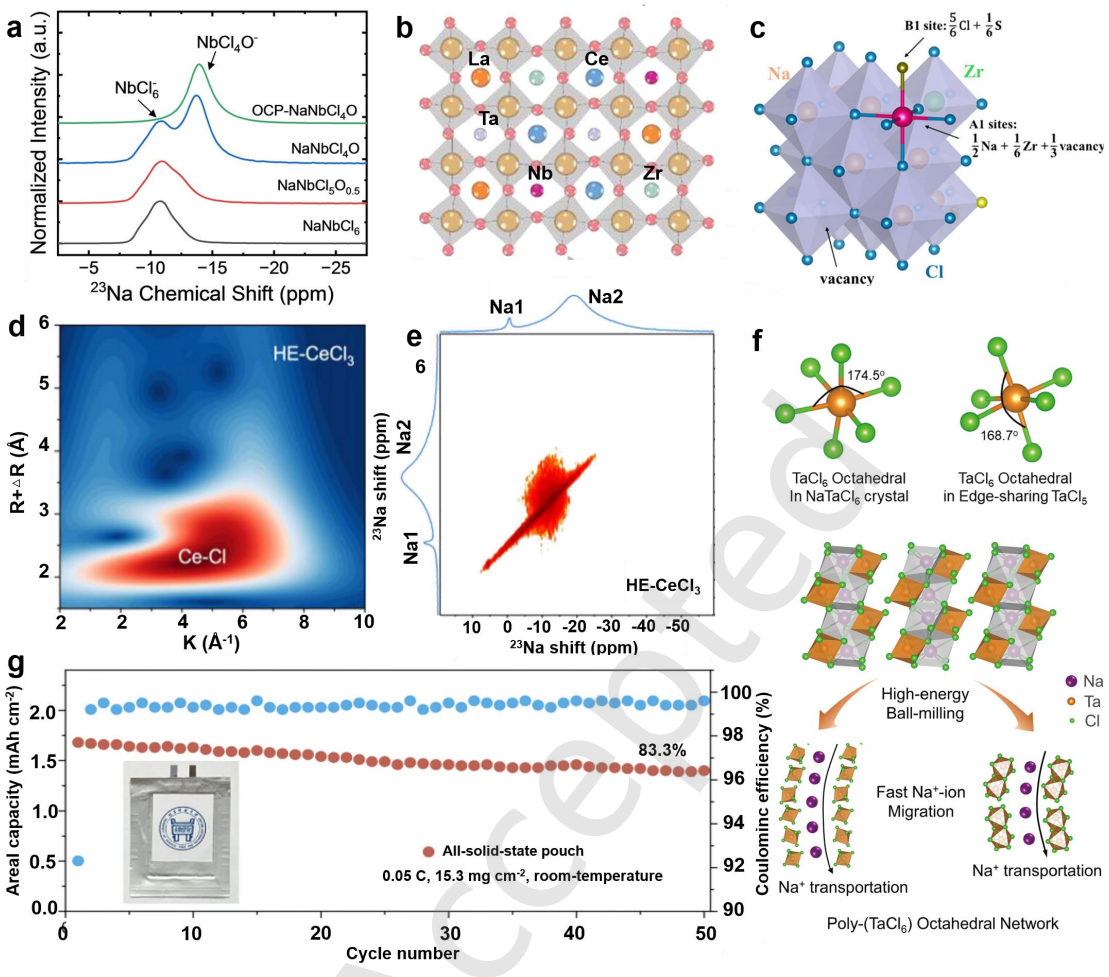


Figure 3 (a) ^{23}Na MAS NMR spectra of the $NaNbCl_{6-2x}O_x$ series. (b) Configurational-entropy design strategy for the $CeCl_3$-based electrolyte. (c) Crystal structure of NZCS. (d) Wavelet-transform extended X-ray absorption fine structure (WT-EXAFS) at the Ce L_3-edge for HE-$CeCl_3$. (e) Two-dimensional ^{23}Na-^{23}Na exchange spectroscopy (EXSY) spectra illustrating intersite Na^+ exchange in the HE-$CeCl_3$ system. (f) Schematic illustration of local-structure reconstruction and Na^+ conduction in amorphous $NaTaCl_6$. (g) Cycling performance of the HE-$CeCl_3$-based pouch-type ASSIB. (a) is adapted with permission from Ref. [30], published by Wiley-VCH; (b,d,e,g) are adapted with permission from Ref. [33], published by Wiley-VCH; (c) is adapted with permission from Ref. [39], published by the American Chemical Society; and (f) is adapted with permission from Ref. [34], published by Elsevier.

High-entropy UCl_3-type halides provide another route by using multication co-occupation to actively increase local structural freedom (Fig. 3b). A representative composition, $NaLa_{0.472}Ce_{0.472}Ta_{0.155}Nb_{0.155}Zr_{0.155}Cl_6$ (HE-$CeCl_3$), retains a powder X-ray diffraction (XRD) pattern that can be refined as a single $P6_3/m$ hexagonal phase [33], showing that the high-entropy composition does not destroy the fundamental long-range topology of the UCl_3-type framework. High-resolution transmission electron microscopy (HRTEM), however, reveals continuous amorphous regions between randomly oriented crystallites, giving rise to a distinct glass-ceramic microstructure. The homogeneous coexistence of Ce, La, Ta, Nb, and Zr on the parent cation sublattice introduces substantial local size mismatch and coordination distortion, broadening the local structural distribution beneath the average crystal structure (Fig. 3d). HRTEM together with high-angle annular dark-field scanning transmission electron microscopy/energy-dispersive X-ray spectroscopy (HAADF-STEM/EDS) further confirms the coexistence of randomly oriented grains and amorphous regions and the homogeneous distribution of multiple metal species, indicating that the disorder reflects local structural heterogeneity embedded within the high-entropy host rather than simple segregation into independent impurity phases. This reconstruction directly affects Na^+ site occupancy and intersite exchange. ^{23}Na MAS NMR shows an increased fraction of the more mobile Na1 sites in HE-$CeCl_3$ accompanied by reduced Na2 occupancy, indicating redistribution of Na^+ from Na2 toward the transport-active Na1 environment. More significantly, two-dimensional ^{23}Na-^{23}Na EXSY shows well-separated Na1 and Na2 signals in the unmodified Na-$CeCl_3$, indicating limited exchange between the two site types, whereas HE-$CeCl_3$ exhibits a broadened and nearly continuous Na1-Na2 exchange-correlation band (Fig. 3e), directly demonstrating intersite exchange between previously more isolated Na^+ environments. Ab initio molecular dynamics (AIMD) simulations further show that compositional disorder and lattice distortion induced

Just Accepted

by multication incorporation regulate local Na^+ coordination, widen migration bottlenecks, and generate a more continuous one-dimensional diffusion pathway along the c axis. Accordingly, HE-$CeCl_3$ reaches a room-temperature ionic conductivity of approximately 1.01×10^{-3} S cm^{-1}, around five orders of magnitude higher than the 3.37×10^{-8} S cm^{-1} of unmodified Na-$CeCl_3$, while the activation energy decreases to 0.27 eV. Its electronic conductivity remains only 4.2×10^{-10} S cm^{-1}, and the oxidative stability extends to approximately 4.46 V versus Na/Na^+. The significance of this system also extends beyond transport. HE-$CeCl_3$ tolerates low-polarity solvents such as chlorobenzene, enabling solution casting of dense, self-supporting composite electrolyte membranes approximately 55 μm thick. After adding polyisobutylene (PIB) binder, the membrane retains a room-temperature ionic conductivity of 2.1×10^{-4} S cm^{-1}. This wet-processing route enables pouch-type ASSIBs using an NVOPF composite cathode with an areal loading of 15.3 mg cm^{-2}, an HE-$CeCl_3$/NPS bilayer electrolyte membrane, and a Na-Sn anode (Fig. 3g). The pouch cell delivers an initial areal capacity of 1.7 mAh cm^{-2} at room temperature and retains 83.3% capacity after 50 cycles at 0.05 C. In conventional pellet cells, HE-$CeCl_3$ also supports 600 cycles of an NVOPF cathode at 0.3 C with 88.3% capacity retention and an areal capacity of approximately 2.8 mAh cm^{-2} under high-loading conditions.

In contrast to the high-entropy strategy, which increases local structural freedom while preserving the average UCl_3-type framework, $NaTaCl_6$ demonstrates a more complete disordering pathway (Fig. 3f) [34]. Without changing the nominal composition, high-energy mechanochemical treatment progressively disrupts long-range periodicity and reconstructs the local coordination network in the amorphous state. Crystalline $NaTaCl_6$ adopts a $P2_1/n$ monoclinic structure in which Na^+ fully occupies specific crystallographic sites and intrinsic ion transport is limited. During prolonged high-energy ball milling, the room-temperature conductivity increases within the first 40 h from 6×10^{-5} to 4×10^{-3} S cm^{-1}, while the characteristic diffraction peaks broaden and nearly disappear and the Na^+ migration activation energy decreases from approximately 0.41 to 0.30 eV. Re-annealing the highly conductive sample to recover crystallinity reduces the conductivity by approximately 2-3 orders of magnitude. The local structure does not become fully random when long-range order is lost. Na K-edge XAS shows reduced local symmetry and weaker Na-Cl interactions as milling proceeds and conductivity increases, whereas Ta L_3-edge extended X-ray absorption fine structure (EXAFS) and Raman measurements reveal increasing distortion and closer approach of $TaCl_6$ octahedra, ultimately producing a reconstructed poly-($TaCl_6$) network. This local structural reorganization is associated not only with high bulk transport but also with favorable cathode-side electrochemical performance. An ASSIB using $Na_3V_2(PO_4)_3$ as the cathode retains approximately 98% of its capacity after 1500 cycles at 0.5 C and room temperature, while the average Coulombic efficiency reaches 99.98% over 600 cycles at 1 C. Even after 4000 cycles at 60 °C and 3 C, approximately 81% of the capacity is retained.

Taken together, these studies show that structural design in sodium halides has progressively shifted from the average long-range structure toward increasingly local structural scales. Early design centered on crystal frameworks, migration channels, and vacancy concentrations, and subsequently expanded to metastable Na^+ sites and the spatial organization of defects. Mixed-anion and multicomponent chemistries then pushed the design space into the first coordination shell, metal-anion connectivity, and correlations among distinct local units. Meanwhile, nanocrystalline-amorphous coexistence, glass-ceramic structures, and fully amorphous systems demonstrate that long-range periodicity is no longer a prerequisite for constructing fast ion-transport networks. The descriptors used for high-performance sodium halides have accordingly evolved from space group, lattice parameters, and average vacancy concentration toward local coordination, site-energy distributions, short-range connectivity, and structural heterogeneity. This conceptual shift provides the basis for directly treating amorphous structure as a design target.

3 Structural Construction and Chemical Regulation of Amorphous Sodium Halides

Unlike crystalline electrolytes, amorphous sodium halides lack long-range periodicity but retain local coordination structures that can be regulated through composition and synthesis. Understanding how these local structures form and evolve is therefore essential for designing highly conductive amorphous electrolytes. Once long-range periodicity is no longer treated as a prerequisite for materials design, the compositional space and local structural degrees of freedom of sodium halides expand substantially. An amorphous state, however, does not correspond to a unique structure. Stoichiometric deviations during mechanochemical reactions, the coordination preferences of different cations or anions, and kinetic competition during melt cooling can all alter the final crystallite size and local connectivity. Existing studies have generated a continuum of structures ranging from nanocrystalline/amorphous coexistence and glass ceramics to nearly fully amorphous states, with no simple one-to-one relationship between crystallinity and ionic transport, electrochemical stability, or processability. Accordingly, design of amorphous sodium halides is moving from simply “breaking the lattice” toward active control of nonequilibrium structure formation and the resulting local chemical environments.

3.1 Amorphization and Regulation of Structural Order

Mechanochemical treatment is one of the most common routes to amorphization in sodium halides, but ball milling alone does not uniquely determine the final structural state. The Na-Y-Zr-Cl system provides a clear example (Fig. 4a). At fixed Y/Zr ratio, progressively reducing the NaCl content in $Na_{2.25-x}Y_{0.25}Zr_{0.75}Cl_{6-x}$ drives a transition from fine nanocrystals toward an amorphous state [36]. Samples with x = 1.375 and 1.625 still show refined diffraction rings in selected-area electron diffraction

Under Review

(SAED), whereas x = 2.000 is dominated by a diffuse halo, indicating near-complete loss of long-range order with only short-range structure remaining. NaCl deficiency simultaneously alters the population of Na^+ environments: prismatic Na sites are present across the composition range in ^{23}Na NMR, whereas octahedral Na environments occur mainly at higher Na content. Composition therefore couples crystallite size, vacancy concentration, and local Na coordination. Importantly, the highest conductivity in this series is not found at the fully amorphous end member. $Na_{0.625}Y_{0.25}Zr_{0.75}Cl_{4.375}$ (x = 1.625) reaches approximately 4.0 × 10^{-4} S cm^{-1} at room temperature, whereas further NaCl removal increases the amorphous character but lowers the conductivity. The authors attribute this non-monotonic behavior to a balance between the number and mobility of mobile Na^+ carriers: high vacancy concentrations favor migration, but excessive Na deficiency reduces the number of charge carriers. Thermal treatment provides a more direct comparison. After crystallization at 100 °C, the x = 1.625 and 2.000 samples redistribute Na^+ from prismatic toward more octahedral environments, accompanied by an approximately one-order-of-magnitude decrease in ionic conductivity and an increase in activation energy. Thus, nanocrystalline fraction, amorphous fraction, defects, and local Na sites are interdependent structural variables rather than independently tunable parameters.

The influence of composition on amorphous-forming tendency becomes even more evident in multication chlorides. Under identical mechanochemical treatment, increasing the Ta^{5+} fraction in $Na_{2-x}Zr_{1-x}Ta_xCl_6$ progressively weakens the Bragg reflections, and $Na_{1.4}Zr_{0.4}Ta_{0.6}Cl_6$ (x = 0.6) is nearly devoid of long-range periodicity [35]. Further increasing the Ta content, however, causes crystalline $NaTaCl_6$ features to re-emerge. Ionic conductivity follows the same non-monotonic trend, reaching 1.95 mS cm^{-1} at x = 0.6 with E_a = 0.26 eV, compared with only 1.31 × 10^{-5} S cm^{-1} and E_a = 0.44 eV for crystalline Na_2ZrCl_6 (Fig. 4d). Here, Ta does not simply act as a conventional aliovalent dopant that regulates vacancies. The coexistence of chemically distinct Zr- and Ta-centered coordination units frustrates retention of the parent periodic arrangement and thereby changes the tendency of the system to enter an amorphous state under mechanochemical conditions. The same strategy yields amorphous Hf/Ta- and Nb/Ta-based chlorides with room-temperature conductivities above 10^{-3} S cm^{-1}, demonstrating that cation chemistry itself can serve as a handle for tuning glass-forming tendency without relying on a single specific parent phase [43].

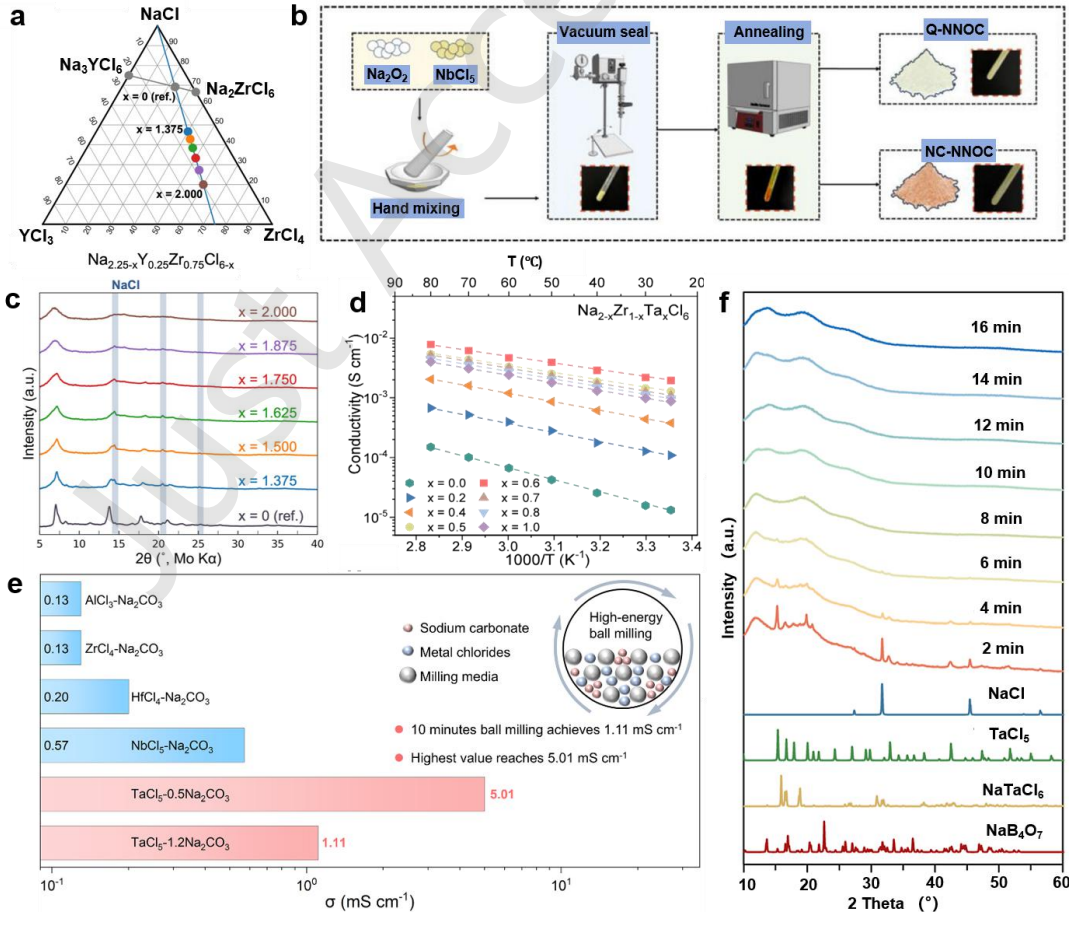


Figure 4. (a,c) Composition-dependent structural evolution and long-range order in the Na-Y-Zr-Cl system. (b) Schematic illustration of the synthesis of rapidly quenched $NaNbOCl_4$ (Q-NNOC) and naturally cooled $NaNbOCl_4$ (NC-NNOC). (d) Arrhenius

Just Accepted

plots for $Na_{2-x}Zr_{1-x}Ta_xCl_6$. (e) Ionic conductivities of representative metal chloride-Na_2CO_3 electrolytes prepared by high-energy ball milling, highlighting the high conductivity achieved in $TaCl_5$-Na_2CO_3 compositions. (f) Time-resolved XRD patterns of NTBOC during mechanochemical milling, showing borate-assisted ultrafast amorphization. (a,c) are adapted with permission from Ref. [36], published by Elsevier; (b) is adapted with permission from Ref. [27], published by Wiley-VCH; (d) is adapted with permission from Ref. [35], published by the American Chemical Society; (e) is adapted with permission from Ref. [31], published by the Royal Society of Chemistry; and (f) is adapted with permission from Ref. [32], published by the American Chemical Society.

Mechanochemistry is not the only route to such nonequilibrium structures. Melt-cooling experiments on $NaNbOCl_4$ separate compositional effects from formation kinetics [27]. When the same melt is naturally cooled over 24 h, local NaCl crystals precipitate, whereas sub-second quenching in less than 2 s suppresses NaCl nucleation and preserves the nearly fully amorphous Q-NNOC phase (Fig. 4b). The corresponding room-temperature conductivity increases from 0.80 mS cm^{-1} for the naturally cooled NC-NNOC to 1.51 mS cm^{-1} for Q-NNOC, while an air-quenched intermediate structure reaches 1.23 mS cm^{-1}; the experimental activation energy decreases from 0.324 to 0.298 eV. Cooling rate determines the extent to which the high-temperature melt can undergo structural relaxation and phase separation, allowing the same stoichiometry to freeze into states with different degrees of short- and long-range order. This kinetic control also affects macroscopic processing properties. After pressing at 300 MPa, Q-NNOC exhibits a porosity of only 5.8%, compared with 14.6% for the naturally cooled sample, while its average Young's modulus is 8.2 GPa versus 12.7 GPa for the latter. An ASSIB assembled with Q-NNOC and a P2-type layered oxide retains 82.61% of its capacity after 250 cycles at 0.5 C, whereas NC-NNOC decays more rapidly under the same conditions. Amorphous-phase formation therefore influences not only bulk ion transport, but also particle densification, interfacial contact, and the mechanical response of the electrolyte in a working cell.

Recent work has begun to exploit reaction chemistry itself to shorten the time required for amorphization. Conventional systems such as $NaTaCl_6$ often require tens of hours of high-energy ball milling, whereas in $TaCl_5$-Na_2CO_3, reaction between carbonate and Lewis-acidic metal chlorides accompanied by CO_2 release markedly accelerates the mechanochemical process [31] (Fig. 4e). $TaCl_5$-$1.2Na_2CO_3$ reaches 1.11 mS cm^{-1} after only 10 min of milling, and optimized $TaCl_5$-$0.5Na_2CO_3$ reaches 5.01 mS cm^{-1} at room temperature with $E_a = 0.316$ eV. A similar acceleration occurs in $Na_{1+x}Ta(B_4O_7)_xCl_{6-x}$ [32]. After $[B_4O_7]^{2-}$ incorporation, diffraction peaks from the precursors rapidly disappear within several minutes of ball milling, and the $x = 0.33$ composition reaches 3.1 mS cm^{-1} within 10 min with an activation energy of approximately 0.28-0.29 eV, whereas $NaTaCl_6$ remains substantially less conductive under the same short milling conditions (Fig. 4f).

These results show that no universal structural threshold defines amorphization in sodium halides; the final degree of order depends strongly on both composition and preparation kinetics. NaCl deficiency, coexistence of dissimilar metals, and rapid quenching can all suppress the establishment of long-range periodicity, whereas carbonate and borate further accelerate amorphous-phase formation by altering mechanochemical reaction pathways. Despite their reduced long-range order, materials obtained through these different routes do not exhibit equivalent Na^+ transport behavior. In Na-Y-Zr-Cl, a nanocrystalline/amorphous coexistence composition provides a more favorable balance between carrier concentration and Na^+ mobility, whereas in Na-Zr-Ta-Cl and rapidly quenched $NaNbOCl_4$, further suppression of crystallization continues to improve ion transport. The performance gain associated with amorphization therefore cannot be described simply as a consequence of "lower crystallinity"; it also depends on the number of Na^+ carriers, defect populations, and the local structures retained during amorphization. Once long-range periodicity is lost, whether local coordination units persist, how they distort, and how they connect become key structural distinctions among amorphous sodium halides.

3.2 Local Coordination and Multiphase Microstructure Design

Loss of long-range order does not erase metal-anion coordination units. Instead, XAS, PDF analysis, Raman spectroscopy, and solid-state NMR across a range of amorphous sodium halides show that local polyhedra generally persist, although their coordination numbers, distortion, and interconnectivity are no longer constrained by a periodic lattice. In amorphous $Na_{1.4}Zr_{0.4}Ta_{0.6}Cl_6$, for example, $[ZrCl_6]^{2-}$ and $[TaCl_6]^-$ remain the dominant local structural units, while Ta-centered octahedra show more pronounced geometric distortion. EXAFS can even resolve nearest-neighbor Ta-Ta correlations, demonstrating that short-range metal correlations persist within the amorphous matrix [35]. The structural freedom of the amorphous state therefore arises primarily from the loss of uniform orientational and connectivity constraints among local units rather than from complete randomization of all bonding relationships.

Oxygen incorporation further enriches this local connectivity, and identical chemical compositions can develop markedly different short-range structures depending on the manner in which local units are connected. Rapidly quenched $NaNbOCl_4$ provides a representative example (Fig. 5a)[27]. Although naturally cooled NC-NNOC has already lost complete long-range periodicity, its PDF retains strong local correlation peaks at $r < 5$ Å, indicating substantial short-range order within the amorphous matrix. Structural models are dominated by corner-sharing NbO_2Cl_4 octahedra linked through bridging oxygen atoms to form Nb-O-Nb chain-like motifs with partial continuity and directionality, with Nb-O-Nb and O-Nb-O bond angles concentrated near 180° and 90°, respectively. By contrast, the short-range PDF peaks of Q-NNOC are further weakened, showing that sub-second quenching not only suppresses NaCl crystallization but also substantially reduces the local structural coherence of the amorphous matrix. This short-range disorder can be

Just Accepted

traced to oxygen connectivity and reconstruction of Nb-centered polyhedra. O 1s X-ray photoelectron spectroscopy (XPS) shows that rapid quenching cleaves part of the Nb-O-Nb bridging oxygen network and increases the fraction of non-bridging oxygen. Wavelet-transform EXAFS (WT-EXAFS) concurrently shows pronounced attenuation of high-R structural correlations and enhancement of local low-R signals, indicating a more complex near-neighbor environment after disruption of extended connectivity. EXAFS fitting yields average Nb-Cl and Nb-O coordination numbers of approximately 3.7 and 1.8 in Q-NNOC. These noninteger values further demonstrate that the local environment around Nb cannot be represented by a single idealized NbO_2Cl_4 configuration, but instead comprises a distribution of O/Cl coordination numbers and connection modes. Consistently, computational models show that cleavage of bridging O disrupts continuous Nb-O-Nb connections, producing substantial misalignment, connectivity breaks, and broadened bond-length and bond-angle distributions among NbO_2Cl_4 polyhedra. Continuous symmetry measure (CSM) analysis likewise indicates larger octahedral distortion and lower local coordination symmetry in the quenched structure. Thus, cooling kinetics in $NaNbOCl_4$ regulate not merely the "degree of amorphization," but more fundamentally the manner in which the same class of Nb-centered coordination units connect within the amorphous matrix. Natural cooling preserves more bridging-O-mediated polyhedral connections and therefore more directionally correlated chain-like motifs, whereas rapid quenching increases non-bridging oxygen, interrupts Nb-O-Nb bridges, and enhances octahedral distortion, transforming relatively regular connections into a broader distribution of coordination and orientation states. Consequently, the O/Cl ratio or average Nb-O coordination number alone is insufficient to characterize the local structure of an oxychloride; whether oxygen is bridging or non-bridging, whether neighboring polyhedra remain continuously connected, and the degree of orientational coherence among these connections are equally important variables distinguishing different amorphous states.

The $NaNbOCl_4$ results show that the role of oxygen in amorphous local structure depends not only on whether O enters the first coordination shell, but also on its specific connectivity. Building on this concept, oxygen-containing polyanions with distinct chemical reactivity and geometry provide additional structural freedom for regulating Ta-centered coordination networks. Different precursors, however, do not participate in amorphous-network formation in the same way. In $TaCl_5$-Na_2CO_3, carbonate is strongly reactive during mechanochemical processing [31]. At low Na_2CO_3 contents, it largely decomposes with CO_2 release and the remaining O enters the first coordination shell of Ta; with increasing Na_2CO_3 content, part of the carbonate can be retained and participate in Ta-O coordination. Fourier-transform infrared (FTIR) spectroscopy identifies Ta-O-Ta bridging motifs (Fig. 5b), while EXAFS gives an average O coordination number of approximately 1.3 together with two distinct Ta-Cl environments, reflecting substantial first-shell distortion (Fig. 5c). Combined PDF analysis, time-of-flight secondary-ion mass spectrometry (ToF-SIMS), and calculations further show that TC-NCO contains both five-coordinate trigonal-bipyramidal and six-coordinate octahedral Ta-centered units. These units can occur in isolation or connect through bridging oxygen to form dimers and larger local aggregates (Fig. 5f), while Na^+ occupies a range of $[NaO_xCl_y]$ environments with coordination numbers of approximately 5-8. In this system, carbonate therefore primarily reconstructs the original Ta-Cl network through reaction-induced decomposition and oxygen incorporation, effectively reshaping the connectivity of the amorphous network [44].

In contrast to carbonate, which reconstructs the local network mainly through reactive decomposition and oxygen transfer, borate retains more distinct polyanionic-unit characteristics in the final amorphous structure. In $Na_{1+x}Ta(B_4O_7)_xCl_{6-x}$, $[B_4O_7]^{2-}$ does not primarily act by complete decomposition and O release; instead, it directly enters the first Ta coordination shell through bridging oxygen and forms mixed $[TaO_xCl_y]$ polyhedra [32]. PDF and EXAFS analyses yield average Ta-O and Ta-Cl coordination numbers of approximately 1.1 and 3.8, with corresponding bond lengths of approximately 1.88 and 2.36 Å (Fig. 5e). Despite substantial local coordination distortion, the overall topology of the Ta-centered framework retains some similarity to that of $NaTaCl_6$. More importantly, embedding $[B_4O_7]^{2-}$ units whose size, charge, and geometry differ strongly from those of Cl^- disrupts uniform orientational relationships among neighboring polyhedra and thereby promotes loss of long-range order. Borate thus provides a route to increasing local configurational freedom through the direct incorporation of retained, chemically distinct polyanionic units.

F^- illustrates a different balance in mixed-anion design. Its high electronegativity and strong M-F bonding generally favor oxidative stability, but strong Na-F electrostatic interactions can also restrict Na^+ migration [45]. In $Na_{0.5}ZrCl_4F_{0.5}$, F does not form a regular independent fluoride framework. Instead, it enters the first coordination shell of Zr to generate mixed-anion $[ZrCl_xF_y]$ polyhedra. X-ray absorption near-edge structure (XANES)/EXAFS measurements show that the initially split Zr-Cl coordination features become broadened and more averaged after F incorporation, while ^{23}Na NMR indicates an increased fraction of prismatic Na and enhanced disorder around Zr sites. Longer Na-F distances introduced by partial F substitution can weaken local Na-anion interactions, whereas excessive F re-establishes stronger local binding [46]. The structural and transport responses therefore exhibit a clear compositional window.

In Review

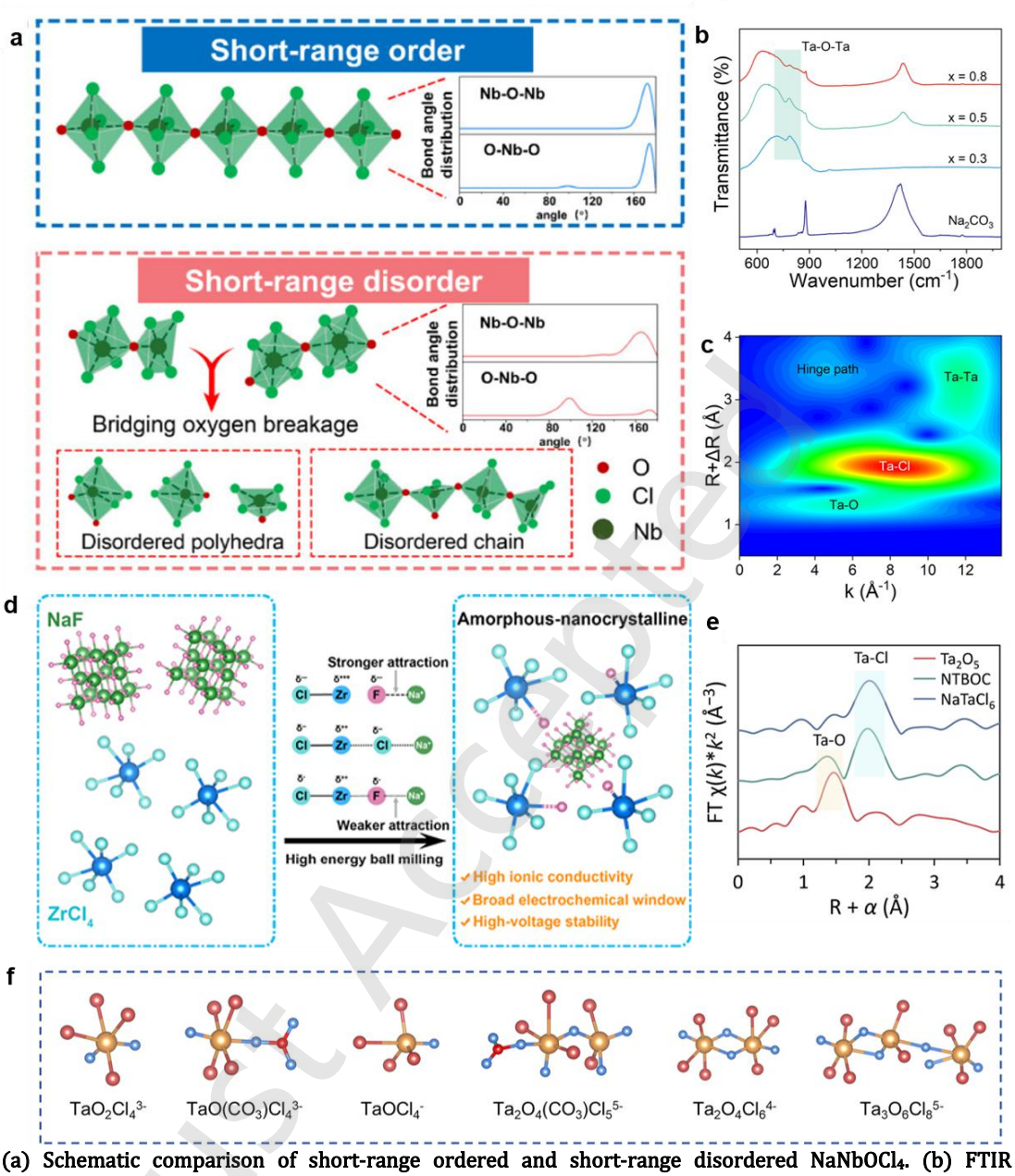


Figure 5. (a) Schematic comparison of short-range ordered and short-range disordered $NaNbOCl_4$. (b) FTIR spectra of $TaCl_5$-xNa_2CO_3 samples (x = 0.3, 0.5, and 0.8) and Na_2CO_3. (c) Wavelet-transformed Ta L_3-edge EXAFS of the TC-NCO electrolyte. (d) Schematic illustration of high-energy ball-milling-induced formation of an amorphous-nanocrystalline NaF-$ZrCl_4$ heterostructure. (e) K^2-weighted Fourier-transformed EXAFS spectra of NTBOC, $NaTaCl_6$, and Ta_2O_5. (f) Representative Ta-centered local coordination motifs in the carbonate-derived oxychloride system. (a) is adapted with permission from Ref. [27], published by Wiley-VCH; (b,c) are adapted with permission from Ref. [31], published by the Royal Society of Chemistry; (d) is adapted with permission from Ref. [47], published by the American Chemical Society; and (e) is adapted with permission from Ref. [32], published by the American Chemical Society.

This chemistry also illustrates why amorphous materials can be difficult to describe using a single "bulk phase" concept. Some systems are intrinsically heterogeneous across multiple length scales. In 2NaF-$ZrCl_4$, approximately 10.8% NaF nanocrystals are dispersed within a highly disordered Zr-Cl-F matrix, and cryogenic transmission electron microscopy (cryo-TEM) directly reveals nanodomains with NaF (200) lattice fringes adjacent to halo-like amorphous regions [47]. The authors therefore proposed that NaF/amorphous interfaces may contribute to rapid Na^+ transport (Fig. 5d). During annealing, the progressive increase of crystalline NaCl, Na_2ZrCl_6, and related phases is accompanied by a continuous decrease in conductivity, further supporting an important contribution from the highly disordered matrix. The optimized sample exhibits a room-temperature conductivity of 2.35×10^{-4} S cm^{-1} and E_a = 0.28 eV. F incorporation also raises the oxidative onset from approximately 3.95 to 4.32 V and enables a high-voltage NFM cell to retain 81.1% of its capacity after 600 cycles at

Just Accepted

0.2 C.

Structural heterogeneity is even more pronounced in Na-Ta-Cl-O [48]. After Ta_2O_5 addition, all oxygen-containing compositions contain more than 50% amorphous phase, while optimized $Na_{2.25}TaCl_{4.75}O_{1.25}$ contains both tens-of-nanometers NaCl particles and larger Ta_2O_5 particles randomly dispersed within a Na-Ta-Cl-O amorphous matrix. The material reaches a room-temperature ionic conductivity of 2.5 mS cm^{-1} and an electrochemical window of approximately 0.4-4.1 V versus Na^+/Na, while also showing improved pellet formability and mechanical strength relative to $NaTaCl_6$. The study proposes that nanoparticle/amorphous interfaces may contribute to the enhanced conductivity and stability, but direct experiments capable of separating bulk and interfacial Na^+ transport are still lacking. Such composite architectures are therefore best viewed as a promising microstructural design direction rather than as systems in which an interfacial-conduction mechanism has already been conclusively established.

The chemical space of amorphous structures has also expanded from O/F chemistry to softer chalcogenide anions. Incorporating S^{2-} into Ta-Cl networks can generate a range of $[TaCl_xS_y]$ units, including five-coordinate $[TaCl_4S]$, with Na^+ exhibiting a broad coordination-number distribution of approximately 6-8 and increased local structural disorder. Related Hf-S-Cl materials contain multiple connection modes, including Hf-Cl/S edge-sharing, Cl corner-sharing, and isolated Hf-Cl/S units, rather than being limited to the more characteristic bridging-oxygen connectivity found in oxychlorides [38,49].

With these developments, "structural design" in amorphous sodium halides can no longer be summarized by a single measure of crystallinity. Long-range order can be disrupted almost completely while local M-X polyhedra remain; changing the anion chemistry can further reconstruct the coordination numbers, bond lengths, and connection modes of these polyhedra within the nonperiodic framework; and incorporating nanocrystals or secondary phases extends structural heterogeneity to larger length scales. Importantly, these chemical modifications are not used solely to maximize ionic conductivity. Fluorination can improve high-voltage stability, carbonate and borate can drastically shorten the mechanochemical time required for amorphization, and nanoparticle-containing oxychlorides can simultaneously improve formability and electrochemical windows. Amorphization therefore provides a materials platform in which structural freedom can be redistributed among local coordination, network connectivity, microstructure, and interfacial properties [50].

4 Fast Na^+ Transport in Amorphous Structures

Although amorphization can create more diverse local environments for Na^+ migration, it does not necessarily guarantee high ionic conductivity. Understanding why different amorphous electrolytes exhibit distinct transport behaviors requires examining how their local structural units are connected and how the framework responds during ion migration. Amorphization relaxes the strict dependence of ion transport on fixed crystallographic sites and periodic migration pathways and broadens the distribution of coordination environments and local structural connections around Na^+. The resulting transport behavior can no longer be described by a single lattice parameter or a unique migration pathway; instead, it depends on energetic and spatial correlations among a distribution of local configurations. Solid-state NMR, total-scattering measurements, and molecular-dynamics simulations increasingly show that fast Na^+ migration in amorphous sodium halides is closely related to local site distributions, short-range structural connectivity, and framework response. Distinguishing these factors is moving the field beyond the empirical statement that "amorphization enhances conductivity" toward a more explicit understanding of ion transport in the amorphous state [27-29,32,37,51].

4.1 Local Connectivity, Structural Coherence, and Migration Networks

Loss of long-range periodicity substantially expands the local structural space accessible to Na^+ in amorphous sodium halides, but this structural freedom does not automatically translate into fast long-range ion transport. Even when materials are all classified as amorphous, their local polyhedral connectivity, Na^+ coordination environments, and residual short-range structural correlations can differ markedly. Accordingly, whether local structural units achieve sufficient connectivity without rebuilding excessively strong spatial coherence may be more closely related to Na^+ migration than crystallinity alone.

This point is illustrated by comparing amorphous Na_2O_2-MCl_y (M = Hf, Zr, and Ta) dual-anion oxychlorides, here denoted NHOC (M = Hf), NZOC (M = Zr), and NTOC (M = Ta) [28]. Although NHOC, NZOC, and NTOC are all amorphous, their room-temperature ionic conductivities are only 0.52, 0.42, and 2.0 mS cm^{-1}, respectively, with corresponding activation energies of 0.36, 0.35, and 0.30 eV, demonstrating substantial transport differences even after long-range order has disappeared (Fig. 6a). At comparable Na contents, the larger fraction of oxygen corner-sharing units in NTOC is accompanied by stronger Na-site distortion, which the authors associate with more effective Na^+ migration pathways and lower migration barriers. In contrast, the more rigid local structural connections in NHOC and NZOC correspond to lower ion mobility. Thus, even after amorphization has occurred, the connectivity characteristics of local polyhedra can significantly modulate the migration potential-energy landscape experienced by Na^+ (Fig. 6b).

Recent studies of the continuous $NaTaO_xCl_{6-2x}$ compositional series further show that the relationship between local connectivity and Na^+ transport is not simply monotonic [29]. With increasing O^{2-} content, the system evolves from a crystalline structure dominated by isolated $[TaCl_6]$ units toward amorphous oxychlorides. At the intermediate composition x = 0.5, the local structure preferentially contains $[TaOCl_5]$ units and $[Ta_2OCl_{10}]$ dimer-like motifs connected by bridging oxygen; further O^{2-} incorporation leads to increasingly continuous trans-$[TaO_2Cl_4]$ chain motifs (Fig. 6c). In parallel, the

Just Accepted

room-temperature ionic conductivity rises rapidly from approximately 5.2×10^{-2} mS cm^{-1} for $NaTaCl_6$ and reaches approximately 4 mS cm^{-1} near x = 0.5, but does not continue to increase when higher O contents produce a more coherent Ta-O-Ta network (Fig. 6d). This non-monotonic trend demonstrates that although continuous local connections are beneficial for building migration networks, greater structural coherence does not necessarily accelerate Na^+ transport. Atomistic models at x = 0.5 make this distinction particularly clear. Two structures composed of the same $[Ta_2OCl_{10}]$ dimer building blocks show markedly different Na^+ mobility associated with differences in the relative orientations of the dimers. In the lowest-energy aligned configuration, the Ta-O-Ta linkages are strongly parallel, whereas the unaligned configuration retains lower orientational coherence and a more dispersed local arrangement (Fig. 6e). The corresponding orientational distributions show a broad, nearly continuous probability distribution for equatorial ligands in the unaligned configuration but sharply localized regions in the aligned configuration (Fig. 6f). This difference indicates that stronger dimer alignment imposes greater constraints on the accessible orientations of the local framework, whereas the unaligned arrangement preserves a wider range of local configurations. Such orientational freedom may allow the coordination environment surrounding Na^+ and the geometry of nearby migration bottlenecks to accommodate a broader range of structural arrangements, potentially facilitating ion migration. Thus, even when the local connectivity units are identical, the structural coherence arising from their spatial arrangement can substantially change the migration configurations accessible to Na^+. Lower orientational coherence preserves a broader range of local configurational freedom, whereas highly regular dimer alignment reintroduces structural constraints. In this context, structural coherence describes the degree of orientational correlation among neighboring structural units, while configurational freedom refers to the range of local arrangements accessible within the framework. These results clarify the distinction between "local connectivity" and "structural coherence": completely isolated polyhedra cannot provide continuous migration networks, yet local connections that evolve into highly ordered correlated structures can likewise restrict configurational accessibility. The advantage of x = 0.5 therefore does not arise simply from the formation of O-bridged dimers, but from the ability of these locally connected units to retain limited long-range and orientational coherence within the amorphous matrix, balancing migration-network continuity with local configurational diversity.

Just Accepted

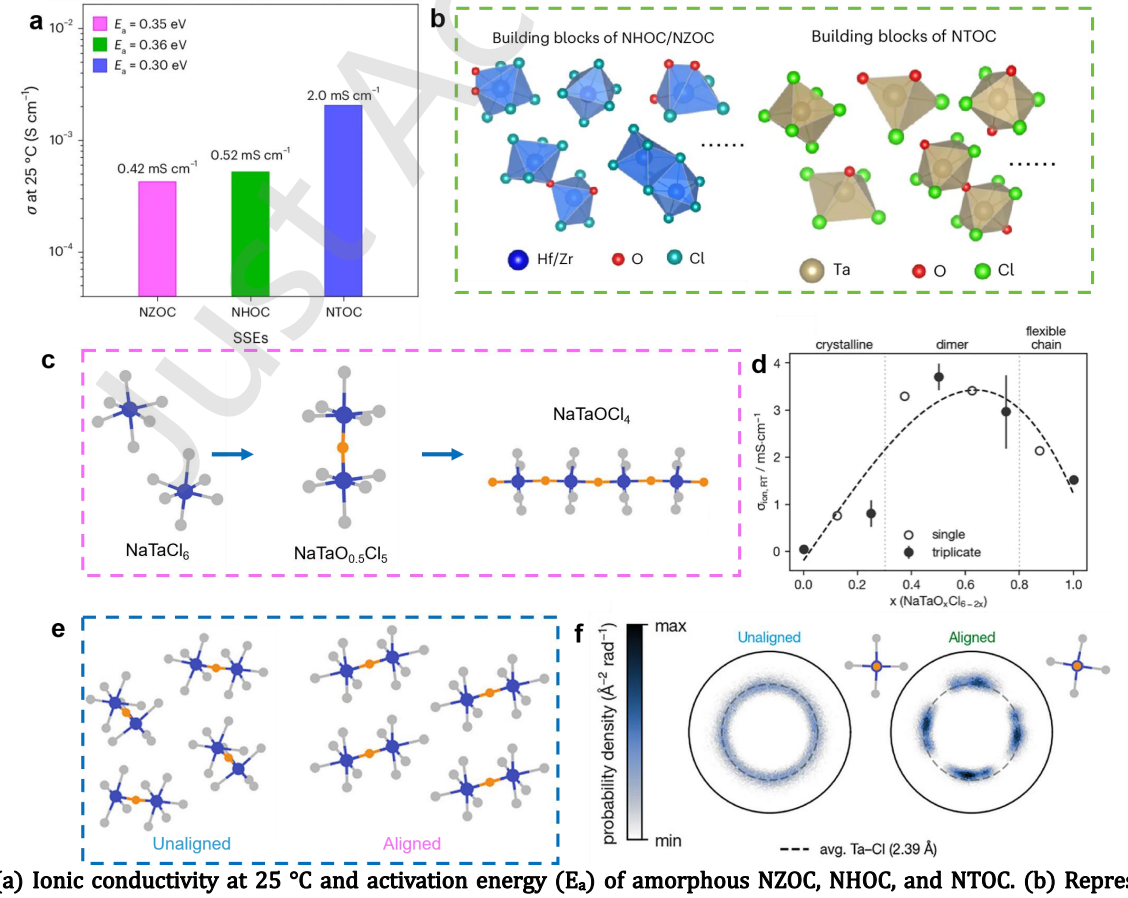


Figure 6. (a) Ionic conductivity at 25 °C and activation energy (E_a) of amorphous NZOC, NHOC, and NTOC. (b) Representative local building blocks in NHOC/NZOC and NTOC. (c) Composition-dependent evolution of local motifs from isolated $[TaCl_6]$ units

to O-bridged dimers and chain-like $NaTaOCl_4$ motifs. (d) Room-temperature ionic conductivity of $NaTaO_xCl_{6-2x}$ as a function of oxygen content x, showing a non-monotonic dependence on connectivity. (e) Unaligned and aligned [Ta_2OCl_{10}] dimer configurations at x = 0.5. (f) Probability-density maps of equatorial Cl-ligand orientations about the Ta-O axis; the unaligned configuration exhibits a broader accessible orientational distribution, whereas the aligned configuration is more localized. (a,b) are adapted with permission from Ref. [28], published by Springer Nature; and (c–f) are adapted with permission from Ref. [29], published by Wiley-VCH.

A similar effect is found in $NaNbOCl_4$ samples with different degrees of short-range order [27]. Although both Q-NNOC and NC-NNOC have lost complete long-range periodicity, their Na^+ transport remains markedly different, showing that residual short-range correlations can still regulate the local migration potential-energy landscape even after the overall structure is highly disordered. Weakening local binding can also coincide with enhanced migration-network connectivity. In $Na_{1+x}Ta(B_4O_7)_xCl_{6-x}$, for example [32], borate incorporation lowers the average Na^+ coordination number and expands the accessible three-dimensional migration region, further illustrating that a large number of local configurations in an amorphous structure can contribute to long-range rapid diffusion only when they are effectively connected in space.

Overall, fast Na^+ transport in amorphous sodium halides does not arise from independently maximizing either the degree of disorder or network connectivity. Instead, it depends on balancing local connectivity, structural coherence, and configurational freedom. Moderate local connectivity allows low-barrier migration configurations to connect spatially, while limited structural coherence helps prevent excessively strong spatial correlations from narrowing the range of accessible configurations. In structurally flexible systems, these static differences can further influence the instantaneous response of the framework during ion migration.

4.2 Coupling between Framework Dynamics and Na^+ Migration

Static local disorder is not the only structural degree of freedom that can participate in transport in amorphous halides. Because halide frameworks are relatively soft, metal-anion polyhedra can undergo pronounced libration, reorientation, and even rotation during thermal motion. When such motion occurs near a Na^+ migration bottleneck, it can transiently modify local coordination and channel geometry [32,37,38].

A comparison between $NaTaCl_6$ and $NaNbCl_6$ provides some of the most systematic evidence for such cation-anion coupling [37]. In AIMD simulations, [$TaCl_6$] polyhedra in $NaTaCl_6$ undergo persistent and pronounced reorientation, whereas the orientational changes of [$NbCl_6$] are substantially more restricted (Fig. 7a,b). Representative local trajectories further show that polyhedral reorientation can occur concurrently with displacement of neighboring Na^+ ions, while Na^+ motion remains more localized in the system with restricted framework dynamics (Fig. 7e,f). Framework motion also directly alters the migration geometry experienced by Na^+. For example, the local Cl-defined bottleneck expands markedly during [$TaCl_6$] reorientation, whereas the corresponding change in $NaNbCl_6$ is much smaller (Fig. 7c). The characteristic Na^+ residence-correlation times are approximately 15.2 and 23.4 ps, respectively, indicating faster escape of Na^+ from its local coordination environment in $NaTaCl_6$, and the polyhedral orientational correlation likewise decays more rapidly in $NaTaCl_6$. More importantly, the joint correlation describing Na^+ translation together with polyhedral orientational changes yields characteristic times of approximately 9.6 ps for $NaTaCl_6$ and 16.3 ps for $NaNbCl_6$, both shorter than the corresponding individual Na residence and polyanion orientational correlations (Fig. 7g). These results indicate that Na^+ escape from the local coordination cage and polyhedral reorientation are not independent on the relevant time scale. Long-time deep-potential molecular dynamics (DPMD) simulations extend this distinction to room temperature: during 10 ns simulations at 300 K, Ta-Cl bonds in ordered $NaTaCl_6$ mainly undergo small-amplitude librations around their equilibrium directions, whereas clear [$TaCl_6$] rotation emerges in disordered $NaTaCl_6$.

Mixed-anion chemistry can further modify framework dynamics. In $0.5Na_2S$-$TaCl_5$, S^{2-} incorporation weakens and softens the Ta-Cl/S framework, giving local polyhedra a greater capacity for structural response [38]. The authors propose that a softer anionic framework can adjust local coordination geometry through local relaxation as Na^+ approaches a migration bottleneck, thereby reducing the structural penalty required for Na^+ to cross a transient barrier relative to a rigid framework (Fig. 7j). In contrast to the $NaTaCl_6$ study, however, this system does not yet provide direct conditional-hopping statistics such as $\nu_{hop}|_{rot}$. It therefore provides cross-chemical-system support for an association between enhanced framework dynamics and fast Na^+ diffusion rather than evidence of equivalent causal strength.

Borate incorporation affects both static local structure and dynamic response. In $Na_{1+x}Ta(B_4O_7)_xCl_{6-x}$, $[B_4O_7]^{2-}$ substantially reconstructs Ta- and Na-centered coordination environments and generates a broader range of mixed [$TaCl_xO_y$] and [$NaCl_xO_y$] local configurations (Fig. 7i) [32]. At the same time, the characteristic dimensions of Na^+-accessible channels increase, indicating that weakened local coordination and expanded migration space can occur concurrently (Fig. 7h). AIMD simulations further show that borate incorporation enhances local polyhedral reorientation dynamics. Within time windows containing polyhedral reorientation events, the conditional Na^+ hopping frequency $\nu_{hop}|_{rot}$ is substantially higher than the trajectory-averaged hopping frequency ν_{hop} (Fig. 7d), providing a direct dynamic correlation between framework reorientation and Na^+ hopping. Fast transport in this system is therefore better interpreted as the combined outcome of coordination weakening, migration-space expansion, and dynamic framework response rather than as the result of a single paddle-wheel mechanism.

Just Accepted

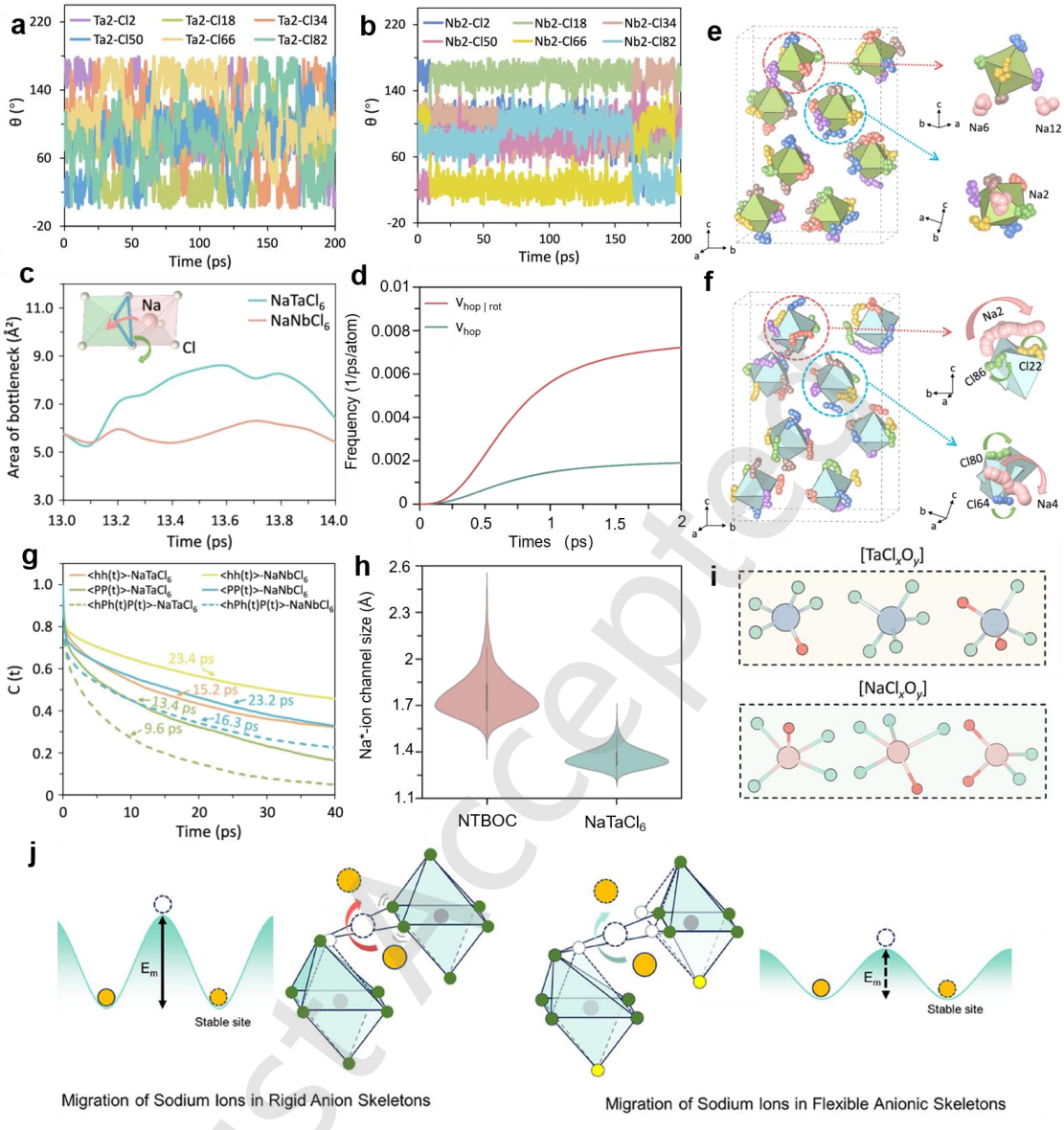


Figure 7. (a,b) Time evolution of the six M-Cl bond orientations for representative [$TaCl_6$] and [$NbCl_6$] polyanions, illustrating their distinct reorientation dynamics. (c) Temporal evolution of the trigonal Na^+ migration bottleneck area in $NaTaCl_6$ and $NaNbCl_6$. (d) Average Na^+ hopping frequency (ν_{hop}) and conditional hopping frequency ($\nu_{hop|rot}$) in NTBOC for hopping events near rotating [$TaCl_xO_y$] units with a 40° rotational cutoff. (e,f) Representative AIMD trajectories of [$TaCl_6$]/[$NbCl_6$] ligands and neighboring Na^+ ions in $NaTaCl_6$ and $NaNbCl_6$. (g) Na^+ residence, polyanion orientational, and joint time-correlation functions for $NaTaCl_6$ and $NaNbCl_6$. (h) Comparison of Na^+ transport-channel sizes in NTBOC and $NaTaCl_6$. (i) Representative distorted [$TaCl_xO_y$] and [$NaCl_xO_y$] coordination environments in NTBOC. (j) Schematic comparison of Na^+ migration in rigid and flexible anionic skeletons. (a–c, e–g) are adapted with permission from Ref. [37], published by Springer Nature; (d,h,i) are adapted with permission from Ref. [32], published by the American Chemical Society; and (j) is adapted with permission from Ref. [38], published by Wiley-VCH.

At present, the most direct quantitative correlations between Na^+ hopping and polyanion reorientation are found primarily in Ta/Nb-based halide/oxyanion systems such as $NaTaCl_6$/$NaNbCl_6$ and NTBOC. In these systems, time-correlation functions and conditional-hopping statistics can directly connect polyhedral reorientation with migration of neighboring Na^+ ions. By contrast, sulfo-halide systems currently provide stronger evidence for the coexistence of framework softening, reorientation, and rapid diffusion than for an equally direct conditional relationship. Existing results therefore do not justify a universal paddle-wheel mechanism for all highly conductive amorphous sodium halides. A more general interpretation is that the amorphous state expands the accessible local structural space and that fast Na^+ transport emerges from the combined effects of a static energy landscape and dynamic structural response: the former determines the low-energy local configurations

Just Accepted

and connected networks available for migration, whereas the latter can further modulate transient bottlenecks and coordination stability during transport.

Table 1. Representative room-temperature ionic conductivities, activation energies, structural states, and design strategies of amorphous or highly disordered sodium halide solid electrolytes.

Composition	Structural state	σ_{RT} (mS cm^{-1})	E_a (eV)	ESW (V)	Design strategy
NaF–AlF_3 [17]	DH	0.0654*	0.308	1.20-4.10	Mesoporous AlF_3 heterostructure
$NaNb_{1.07}Cl_{4.35}O$ [21]	Predom. A	1.02*	0.23	3.15-4.30	O/Cl anion mixing
Q-$NaNbOCl_4$ [27]	A	1.51	0.298	NR-4.43	Short-/long-range disorder
Q-$NaTaOCl_4$ [27]	A/disordered	7.2	-	NR	Rapid-quench disorder
Na_2O_2–$TaCl_5$ [28]	A	2.0	0.30	2.24-4.01	Dual-anion oxychloride
Na_2O_2–$HfCl_4$ [28]	A	0.52	0.36	1.83-4.03	Dual-anion oxychloride
Na_2O_2–$ZrCl_4$ [28]	A	0.42	0.35	1.97-3.94	Dual-anion oxychloride
$NaTaO_{0.5}Cl_5$ [29]	A	4.0	0.31	NR	Disordered local connectivity
$TaCl_5$–0.5Na_2CO_3 [31]	A	5.01	0.316	2.50-4.24	Carbonate-assisted amorphization
$NbCl_5$–Na_2CO_3 [31]	A	0.57	-	2.96-4.17	Carbonate-assisted amorphization
$HfCl_4$–Na_2CO_3 [31]	A	0.2	-	2.02-4.31	Carbonate-assisted amorphization
$Na_{1.33}Ta(B_4O_7)_{0.33}Cl_{5.67}$ [32]	Predom. A	3.1	0.28	2.42-4.07	Borate-induced amorphization
$NaTaCl_6$ [34]	A	4.0	0.30	2.50-4.00	Mechanochemical amorphization
$Na_{1.4}Zr_{0.4}Ta_{0.6}Cl_6$ [35]	A	1.95	0.26	2.38-3.91	Cation coordination disorder
$Na_{0.625}Y_{0.25}Zr_{0.75}Cl_{4.375}$ [36]	NC + A	0.40	0.35–0.37†	NR	NaCl deficiency
0.5Na_2S–$TaCl_5$ [38]	A	2.12*	0.274	2.25-3.89	S/Cl anion dynamics
$Na_{0.5}ZrCl_4F_{0.5}$ [45]	A–NC	0.112	-	NR	Fluorination-induced amorphization
2NaF–$ZrCl_4$ [47]	A–NC	0.235	0.28	1.88-4.32	F-induced disorder
$Na_{2.25}TaCl_{4.75}O_{1.25}$ [48]	A + NPs	2.5	0.33	NR	Nanoparticle-containing oxychloride
Na_2S–1.3$HfCl_4$ [49]	Predom. A	0.452	0.384–0.428†	NR	Chalcohalide mixed anions
$Na_{0.8}Zr_{0.8}Ta_{0.2}Cl_{4.2}F_{0.8}$ [52]	Predom. A	1.02*	0.322	1.72-4.50	Zr-rich F/Cl dual anion
Na_2S–3.3$ZrCl_4$ [53]	Predom. A	0.489	0.351	NR	Tunable S/Cl ratio

A, amorphous; NC, nanocrystalline; NPs, nanoparticles; DH, disordered heterostructure. *Conductivity measured at 30 °C; †E_a represents the reported range for the corresponding compositional series; ESW represents the electrochemical stability window; NR represents data not reported in the original literature.

5 Summary and Outlook

This Mini Review has traced the evolution of sodium halide SSEs from crystalline frameworks toward local disorder and amorphous structures, focusing on structural regulation and its relationship with Na^+ transport. Early studies relied primarily on well-resolved crystal structures and improved ion transport through regulation of site occupancy, vacancy concentration, aliovalent substitution, and migration pathways. With the development of mechanochemical synthesis, mixed-anion chemistry, and multicomponent design, the accessible structural space expanded from periodic lattices to nanocrystalline-amorphous coexistence and fully amorphous states. The structural scales relevant to Na^+ transport consequently broadened from lattice parameters and average occupancies to local coordination, polyhedral connectivity, short-range order, and framework dynamics.

Current evidence shows that amorphization itself is not

Just Accepted

sufficient for high ionic conductivity. Sodium halides with similar long-range disorder can exhibit markedly different Na^+ migration behavior, whereas some systems retaining nanocrystals or appreciable short-range order can also achieve high conductivity. More general structural characteristics are whether local disorder weakens excessively strong Na^+ coordination, reduces energy differences among neighboring migration configurations, and connects low-barrier migration regions into a continuous spatial network. In several Ta/Nb-based halides and oxyhalides, polyanion reorientation also shows explicit temporal correlations with Na^+ hopping, indicating that structural freedom in the amorphous state not only shapes the average migration energy landscape but can also participate in ion transport through transient framework responses. Accordingly, the understanding of amorphous sodium halides is moving beyond the empirical rule that "amorphization promotes conduction" toward a mechanistic description based on local structure, migration networks, and dynamic frameworks.

Despite rapid expansion of the compositional space and substantial improvements in room-temperature ionic conductivity, design of amorphous sodium halides still relies heavily on empirical screening. For practical applications in all-solid-state sodium-ion batteries, ideal halide electrolytes should simultaneously exhibit high Na^+ ionic conductivity, negligible electronic conductivity, sufficient electrochemical stability, favorable mechanical properties, and long-term structural and interfacial stability. These requirements highlight the importance of balancing ion transport performance with structural stability and electrochemical compatibility, rather than pursuing high ionic conductivity alone. Representative ionic conductivities, activation energies, electrochemical stability windows, and major design strategies of amorphous sodium halide electrolytes are summarized in Table 1.

On this basis, several issues merit particular attention:

1. Establish quantitative descriptors for amorphous structures.

Conventional crystallographic parameters can precisely describe unit cells, site occupancies, and defect concentrations, but they are poorly suited to the continuously distributed local environments of amorphous systems. PDF analysis, XAS, solid-state NMR, and molecular dynamics can now provide complementary information on coordination numbers, bond-length distributions, local Na^+ environments, and spatial probability densities, yet the structural parameters used across different studies remain fragmented and no unified set of descriptors is available for comparison across materials. Future work should distinguish long-range disorder, short-range coordination disorder, and local-connectivity disorder and establish quantitative relationships between these structural measures and ion mobility, carrier concentration, and activation energy. Particularly for highly amorphous systems, disappearance of X-ray diffraction (XRD) peaks alone is no longer an adequate structural criterion for explaining performance differences.

In addition, important parameters such as glass transition temperature (T_g), crystallization temperature (T_c), and Na^+ transference number remain insufficiently characterized in many amorphous sodium halide electrolytes. Systematic investigation of these properties, together with local structural characterization and ionic conductivity measurements, could provide deeper insights into the relationships among structural evolution, thermal behavior, and Na^+ transport mechanisms. Future studies should therefore place greater emphasis on the quantitative determination and consistent reporting of these parameters to facilitate meaningful comparisons across different electrolyte systems.

2. Move from "inducing amorphization" to "designing amorphous structures."

Existing studies have shown that Na content deviations, the coexistence of chemically different metals, and anion chemistry involving O^{2-}, F^-, S^{2-}, and borates can strongly alter amorphous formation capabilities, but the amorphous states obtained through these different pathways do not have the same local structure. Therefore, future composition design should focus on the Na^+ coordination environment, metal anion connections, and short-range structure actually generated during the amorphization process, rather than simply pursuing lower crystallinity. In some systems, the highest conductivities do not occur at the most disordered components, suggesting that local structural flexibility, migration network connectivity, and mobile carrier concentration must be balanced. Controlling this balance through composition is critical to moving from empirical amorphization to predictable materials design.

This challenge also involves the formation and stability of the amorphous state. Many high-conductivity materials currently rely on high-energy ball milling or rapid quenching to obtain metastable structures, and their final states are highly sensitive to processing time, energy input, and thermal history. Rather than simply extending grinding times, future efforts should leverage chemistry to lower barriers to glass formation, inhibit detrimental recrystallization, and preserve targeted short-range structures at realistic processing and operating temperatures, thereby improving reproducibility and scalability.

In addition to the initial formation of amorphous structures, their long-term structural stability is equally important to maintain high ionic conductivity. Because many amorphous sodium halide electrolytes are formed under nonequilibrium conditions, long-term storage or electrochemical operations may result in local structural relaxation, short-range order changes, or partial recrystallization. This structural evolution can change the Na^+ coordination environment, redistribute local site energy, and change the connectivity of migration paths, which may affect long-range Na^+ transport and lead to a decrease in conductivity. Therefore, future studies should combine time-dependent ionic conductivity measurements with long-term or operational structural characterization (e.g., XRD, PDF analysis, solid-state NMR, and XAS) to establish quantitative correlations between structural evolution and Na^+ transport behavior.

3. Clarify the causal relationship between static disorder and dynamic transport.

Most current understanding of fast transport in

Just Accepted

amorphous sodium halides remains based on correlations between structural characterization and ionic conductivity. Broad local coordination distributions, flattened energy landscapes, and three-dimensional percolation networks have been observed in multiple systems, but their individual contributions are still difficult to disentangle quantitatively. For framework dynamics, $NaTaCl_6$/$NaNbCl_6$ and NTBOC provide relatively direct temporal-correlation or conditional-hopping evidence linking Na^+ migration with polyhedral reorientation, whereas in many other mixed-anion amorphous systems the role of the dynamic framework is still inferred primarily from rotations, tilts, or local relaxation observed in AIMD. Future work requires experiments and simulations capable of simultaneously resolving Na^+ displacement and framework motion and should move from statistical correlation toward quantitative separation of the contributions of distinct dynamic processes to migration barriers. Only then can concepts such as the paddle-wheel effect, framework softening, and transient bottlenecks evolve from system-specific interpretations into testable structural-design principles.

4. Translate high bulk conductivity into battery-scale performance.

As increasing numbers of amorphous sodium halides reach the 10^{-3} S cm^{-1} conductivity regime, further improvements in bulk conductivity will become as important as interfacial stability, mechanical contact, and processability. Halides often offer advantages on the high-voltage cathode side, but reductive stability against Na metal or Na-Sn anodes remains a widespread challenge. Moisture sensitivity, interfacial contact within composite cathodes, impedance growth during long-term cycling, and ion transport under practical areal capacities can likewise mask the intrinsic advantages of the bulk electrolyte. Future performance evaluation should therefore move beyond room-temperature conductivities measured on pressed powder pellets toward interfacial transport under high active-material fractions, limited external pressure, practical areal capacities, and long-duration cycling. At the same time, rapid mechanochemical synthesis, low-cost precursors, and processing routes compatible with dry-electrode manufacturing will determine whether these amorphous materials can progress from laboratory systems toward scalable ASSIBs [54-58].

5. Expand compositional space and develop predictive design strategies.

The potential of amorphization is not limited to perturbing existing halide lattices. More importantly, it reduces the dependence of fast ion transport on a specific superionic crystal lattice and thereby greatly expands the accessible chemical space. The recently proposed concept of solid dissociation uses weakly interacting halides such as $TaCl_5$, $NbCl_5$, and $ZrCl_4$ as "solid solvents," which undergo local coordination reconstruction with different salts to form amorphous ionic conductors. This strategy has been extended to multiple mobile ions, including Li^+, Na^+, Ag^+, and Cu^+, and 40 of the 73 reported materials exhibit ionic conductivities above 10^{-3} S cm^{-1}. For sodium halides, this concept implies that materials design can move from "identifying and optimizing a specific crystal structure" toward jointly tuning salt-framework interactions, local coordination, and dynamic structural freedom. As the number of candidate metal centers, anions, and salt components grows rapidly, empirical screening alone will become increasingly incapable of covering the enormous amorphous composition space. High-throughput computation, machine learning, and automated experimentation should therefore be combined to predict intermediate structural variables such as amorphous-forming tendency, local coordination distributions, Na^+ site energies, and framework flexibility, rather than fitting ionic conductivity directly, thereby establishing a more physically interpretable composition-local structure-transport predictive framework[59].

6. Resolve short-range order and hidden local structural correlations.

Amorphous or highly disordered structures are not necessarily locally random. Recent work on a spinel-type Li superionic conductor has shown that synchrotron diffuse scattering, three-dimensional difference pair distribution function (3D-ΔPDF) analysis, and Monte Carlo simulations can reveal chemical short-range order (SRO) and local displacements beyond the average structure and connect these structural features to ion transport. For amorphous sodium halides, future studies should distinguish truly random disorder from statistically preferred local connectivity and combine scattering methods with temporal or energy resolution to determine whether short-range correlations represent static glassy disorder or dynamic structural responses associated with Na^+ migration[24].

Overall, the development of amorphous sodium halides is moving materials design away from reliance on specific crystal topologies and toward coordinated regulation of local coordination, structural connectivity, formation kinetics, and dynamic response. Establishing a closed loop among quantitative structural descriptors, reproducible synthesis, and battery-scale validation will be essential for transforming today's high-conductivity materials into a sodium solid-electrolyte platform governed by generalizable design principles and capable of practical implementation.

Declaration of conflicting interests

The authors declare no conflicting interests regarding the content of this article.

Acknowledgements

This work was jointly supported by the National Natural Science Foundation of China (No. U22A20439) and the Natural Science Foundation of Guangdong Province (2024A1515010346).

References

[1] Yang P, Wu Z, Liang Y, et al. Engineering ion transport in all-solid-state sodium-ion batteries: fundamentals, strategies, and perspectives[J]. Progress in Materials Science, 2025, 154: 101503.

Just Accepted

[2] Li X S, Liang J, Cao X, et al. Research progress of inorganic solid electrolyte materials for all-solid-state sodium-ion batteries: X.-S. Li et al[J]. Rare Metals, 2025, 44(5): 2871-2899.
[3] Yang Y, Yang S, Xue X, et al. Inorganic all-solid-state sodium batteries: electrolyte designing and interface engineering[J]. Advanced Materials, 2024, 36(1): 2308332.
[4] Liu K, Ji S, Liu B, et al. Recent advances on coal-based hard carbon anode materials for sodium-ion batteries[J]. Nano Research, 2025, 18(8): 94907625.
[5] Peng B, Wang F, Ahmad N, et al. Volume-complementary bipolar layered oxide enables stable symmetric sodium-ion batteries[J]. Nano Research, 2024, 17(5): 4125-4133.
[6] Pei J, Bai X, Xue P, et al. All-solid-state battery safety in abnormal thermal situations: Crack propagation and lithium dendrite growth[J]. Nano Research Energy, 2025, 4(2): e9120155.
[7] Liu M, Li Y, Guan T, et al. One-step Ta_2O_5-induced amorphization enables improved humid-air tolerance in $NaTaCl_6$-based solid electrolytes for all-solid-state sodium batteries[J]. Journal of Energy Chemistry, 2026. https://doi.org/10.1016/j.jechem.2026.09.004.
[8] Peng T, Ran B, Zhong Y, et al. Machine learning in sodium-ion battery development: Critical perspectives on design innovation and applications[J]. Nano Research Energy, 2026, 5(3): 9120242.
[9] Li Y, Kong S, Guan T, et al. Tailoring Mechanical Compliance and Cycling Stability in Hf-Based Halides for Low-Pressure All-Solid-State Batteries[J]. Nano Energy, 2026: 112520.
[10] Singh K, Chakraborty A, Thirupathi R, et al. Recent advances in NASICON-type oxide electrolytes for solid-state sodium-ion rechargeable batteries[J]. Ionics, 2022, 28(12): 5289-5319.
[11] Xu N H, Li Y J, Hu H Y, et al. Pillar and Pinning Effects in Sodium Oxide Cathodes: Atomic-Level Strategies for Structural Stability[J]. Advanced Functional Materials, 2026, 36(35): e31271.
[12] Akbar M, Moeez I, Kim Y H, et al. Novel Sn-Doped NASICON-Type $Na_{3.2}Zr_2Si_{2.2}P_{0.8}O_{12}$ Solid Electrolyte With Improved Ionic Conductivity for a Solid-State Sodium Battery[J]. Carbon Energy, 2025, 7(5): e717.
[13] Yang H, Weckelmann L, Wu B, et al. Sulfide-Based Electrolytes for All-Solid-State Sodium Batteries[J]. Advanced energy materials, 2026: e05208.
[14] Qiu Y, Xu J. Challenges and prospects for room temperature solid-state sodium-sulfur batteries[J]. Nano Research, 2024, 17(3): 1402-1426.
[15] Fujita Y, Yamanaka R, Suehiro D, et al. Amorphous Sulfide Solid Electrolytes Based on Na_3PS_4–Na_xMO_y (M= P and S) for All-Solid-State Sodium Batteries[J]. ACS Applied Energy Materials, 2025, 8(12): 8216-8223.
[16] Yan B, Kang H, Zhou R, et al. Sodium halide solid electrolytes for all-solid-state sodium batteries: advances, challenges, strategies, and prospects[J]. Energy Storage Materials, 2026: 105042.
[17] Yu Q, Hu J, Xu Y, et al. Mesoporous enhanced heterostructured halide solid electrolytes with high air stability and high abundance for sustainable sodium metal batteries[J]. Angewandte Chemie International Edition, 2025, 64(26): e202425503.
[18] Li Y, Tang X, Li Q, et al. Halide solid-state electrolytes for all-solid-state sodium batteries: progress and perspectives[J]. ACS Energy Letters, 2025, 10(11): 5520-5541.
[19] Schlem R, Banik A, Eckardt M, et al. $Na_{3-x}Er_{1-x}Zr_xCl_{6-A}$ halide-based fast sodium-ion conductor with vacancy-driven ionic transport[J]. ACS Applied Energy Materials, 2020, 3(10): 10164-10173.
[20] Song Y, Zhou H, Zhao T, et al. Inorganic all-solid-state sodium batteries: electrolyte design, interface engineering, and multiscale approaches[J]. Journal of Energy Chemistry, 2026, 112: 415-434.
[21] Tan Y, Gatts J, Fu C, et al. Dual-Anion Sodium Halide-Based Solid Electrolytes with High Ionic Conductivity and High-Voltage Stability[J]. Small, 2025, 21(29): 2504677.
[22] Fu C, Li Y, Xu W, et al. $LaCl_3$-based sodium halide solid electrolytes with high ionic conductivity for all-solid-state batteries[J]. Nature Communications, 2024, 15(1): 4315.
[23] Wang L, Song Z, Lou X, et al. $Na_{2.5}Cr_{0.5}Zr_{0.5}Cl_6$: a new halide-based fast sodium-ion conductor[J]. Small, 2024, 20(28): 2400195.
[24] Chen Y, Ramette C, Krogstad M, et al. Framework Short-Range Order Observed in a Spinel-Type Li Superionic Conductor[J]. Journal of the American Chemical Society, 2026, 148(9): 9244-9254.
[25] Park B J, Kim J S, Kim Y, et al. Ionic Transport Enhancement from Schottky Defect Formation in $NaTaCl_6$ Halide Solid Electrolytes[J]. ACS Energy Letters, 2025, 10(9): 4242-4251.
[26] Park J, Son J P, Ko W, et al. NaAlCl4: new halide solid electrolyte for 3 V stable cost-effective all-solid-state Na-ion batteries[J]. ACS Energy Letters, 2022, 7(10): 3293-3301.
[27] Ma C, Yu Z, Fang J, et al. Coupled engineering of short-/long-range disorder in oxyhalides unlocks benchmark sodium superionic conductor[J]. Angewandte Chemie International Edition, 2026, 65: e202518183.
[28] Lin X, Zhang S, Yang M, et al. A family of dual-anion-based sodium superionic conductors for all-solid-state sodium-ion batteries[J]. Nature Materials, 2025, 24(1): 83-91.
[29] Leifeld J, Parsons A C, Morscher A, et al. Disorder-driven fast Na^+ transport: From crystalline to amorphous networks in the mixed-anion NaTaOxCl6−2x oxychlorides[J]. Advanced Energy Materials, 2026, 16(24): e70977.
[30] Kmiec S, Ruoff E, Manthiram A. A New Class of Oxyhalide Solid Electrolytes $NaNbCl_{6-2x}O_x$ for Solid-state Sodium Batteries[J]. Angewandte Chemie International Edition, 2025, 64(5): e202416979.
[31] Wang X, Zhang S, Yue J, et al. A new class of carbonate-oxychloride solid electrolytes for high-performance sodium-ion all-solid-state batteries[J]. Energy & Environmental Science, 2025, 18(22): 9927-9938.
[32] Li R, Wen S, Wang C, et al. Minute-scale ultrafast synthesis of superionic sodium halide-borate electrolytes for solid-state batteries[J]. Journal of the American Chemical Society, 2026, 148(12): 13235-13246.
[33] Wu M, Liu H, Huang Y, et al. High-Entropy Tailored UCl_3-Type Halides With Enhanced Ionic Conduction and

Just Accepted

Stability for All-Solid-State Sodium Batteries[J]. Angewandte Chemie, 2026, 138(24): e3315764.
[34] Hu Y, Fu J, Xu J, et al. Superionic amorphous NaTaCl6 halide electrolyte for highly reversible all-solid-state Na-ion batteries[J]. Matter, 2024, 7(3): 1018-1034.
[35] Wu M, Qi X, Lei P, et al. Coordination-disorder engineering of amorphous halide superionic conductors for long-cycle all-solid-state sodium batteries[J]. ACS Nano, 2025, 19(40): 35740-35751.
[36] Ridley P, Nguyen L H B, Sebti E, et al. Amorphous and nanocrystalline halide solid electrolytes with enhanced sodium-ion conductivity[J]. Matter, 2024, 7(2): 485-499.
[37] Li R, Xu K, Wen S, et al. A sodium superionic chloride electrolyte driven by paddle wheel mechanism for solid state batteries[J]. Nature Communications, 2025, 16(1): 6633.
[38] Shi Z, Wang Y, Sun S, et al. Amorphous sulfo-halide solid electrolytes with enhanced anion dynamics for highly stable all-solid-state sodium batteries[J]. Advanced Energy Materials, 2026, 16(27): e71091.
[39] Guo X, Chen Y, Yu D, et al. Aliovalent anion incorporation in halide Na-ion conductors for enhanced ionic conductivity[J]. ACS Energy Letters, 2026, 11(4): 3242–3249.
[40] Ri T I, Hwang S G, Kim J S, et al. Fast ionic conductivity by thermal treatment with ultralow electronic transport in solid-state electrolyte Na_3YCl_6[J]. Applied Physics Letters, 2025, 127(14): 141902.
[41] Jia S, Guo Y J, Qi X, et al. Prismatic Na-Ion Coordination in the Sulfide-Chloride Solid Electrolyte Enables Fast Na-Ion Transport[J]. Journal of the American Chemical Society, 2026, 148(32): 34748–34757.
[42] Ruoff E, Kmiec S, Manthiram A. Redox-active halide catholytes for enhanced energy density in solid-state sodium batteries[J]. ACS Applied Materials & Interfaces, 2025, 17(12): 18420-18429.
[43] Li L, Deng L, Zhang K, et al. Zr-Doping Induced Complete Amorphization Toward Highly Stable All-Solid-State Sodium Batteries[J]. Advanced Energy Materials, 2025, 15(40): e03595.
[44] Tang L, Jiang L, Huang Y, et al. Dual Oxygen Precursors Boosting the Ionic Conductivity of Glassy Electrolytes for All-Solid-State Sodium Batteries[J]. Advanced Materials, 2026: e74493.
[45] Wu M, Liu X, Liu H, et al. Fluorinated amorphous halides with improved ionic conduction and stability for all-solid-state sodium-ion batteries[J]. Nature Communications, 2025, 16(1): 2808.
[46] Jeon C, Yoo Y, Kwon E, et al. Fluorinated Halide Solid Electrolytes for High-Voltage All-Solid-State Sodium-Ion Batteries Enabling Reversible Oxygen Redox[J]. ACS Energy Letters, 2025, 11(1): 616-624.
[47] Zhou L, Zhang S, Li W, et al. Amorphous-nanocrystalline fluorinated halide electrolytes with high ionic conductivity and high-voltage stability[J]. Journal of the American Chemical Society, 2025, 147(18): 15136-15145.
[48] Motohashi K, Tsukasaki H, Mori S, et al. Fast sodium-ion conducting amorphous oxychloride embedding nanoparticles[J]. Chemistry of Materials, 2024, 36(19): 9914-9921.
[49] Dong Z L, Sourav B, Gan Y, et al. Design of sodium chalcohalide solid electrolytes with mixed anions for all-solid-state sodium-ion batteries[J]. Advanced Functional Materials, 2026, 36(8): e16657.
[50] Zhou, L.; Bazak, J. D.; Li, C.; Nazar, L. F. 4 V Na Solid State Batteries Enabled by a Scalable Sodium Metal Oxyhalide Solid Electrolyte. ACS Energy Letters, 2024, 9, 4093–4101.
[51] Wei, G.; Binci, L.; Ceder, G. Microscopic Mechanisms of Superionic Na-ion Conductivity in Crystalline and Amorphous $NaMOCl_4$ (M = Nb, Ta) Solid Electrolytes. ACS Energy Letters, 2026, 11, 1861–1870.
[52] Singh S, Cui M, Pugazhendi K N, et al. High conductivity Zr-rich sodium fluorochloride catholytes for all solid-state sodium batteries[J]. ACS Energy Letters, 2026, 11(2): 1965-1973.

[53] Dong Z L, Gan Y, Martins V, et al. Novel sulfide-chloride solid-state electrolytes with tunable anion ratio for highly stable solid-state sodium-ion batteries[J]. Advanced Materials, 2025, 37(30): 2503107.
[54] Wu E A, Banerjee S, Tang H, et al. A stable cathode-solid electrolyte composite for high-voltage, long-cycle-life solid-state sodium-ion batteries[J]. Nature communications, 2021, 12(1): 1256.
[55] Oh J A S, He L, Chua B, et al. Inorganic sodium solid-state electrolyte and interface with sodium metal for room-temperature metal solid-state batteries[J]. Energy Storage Materials, 2021, 34: 28-44.
[56] Tian H, Li J, Cai Y, et al. Dendrite-free, interfacially compatible Na_2ZrCl_6 composite halide solid-state electrolyte for solid-state sodium-ion batteries[J]. Journal of Materials Chemistry A, 2025, 13(20): 15178-15188.
[57] Zhou L H, Li B, Li W P, et al. Regulated interface conduction in halide solid electrolyte for all-solid-state sodium batteries[J]. Tungsten, 2026, 8(1): 85-94.
[58] Park J, Han D, Son J P, et al. Extending the electrochemical window of Na^+ halide nanocomposite solid electrolytes for 5 V-class all-solid-state Na-ion batteries[J]. ACS Energy Letters, 2024, 9(5): 2222-2230.
[59] Yue J, Zhang S, Wang X, et al. Universal superionic conduction via solid dissociation of salts in van der Waals materials[J]. Nature Energy, 2025, 10(10): 1237-1250.

Just Accepted



Zhouguang Lu* is Professor in the Department of Materials Science and Engineering at Southern University of Science and Technology, and Fellow of the Royal Society of Chemistry (FRSC). His research focuses on the molecular design, precise synthesis, structural regulation, and electrochemical reaction mechanisms of advanced energy materials. He has published for more than 200 papers with H index of 85.



Huanzhu Lv is currently a third-year Ph.D. candidate at Southern University of Science and Technology. His research focuses on all-solid-state sodium batteries.

Just Accepted